Chemical Engineering Journal 425 (2021) 131472

Contents lists available at ScienceDirect

Chemical Engineering Journal

journal homepage: www.elsevier.com/locate/cej

Post-processing strategies for improving the electrical and mechanical properties of MXenes

Hao Tang [a,b], Ranran Wang [a,c,*], Liangjing Shi [a], Evgeniya Sheremet [d], Raul D. Rodriguez [d,*], Jing Sun [a,*]

[a] The State Key Lab of High Performance Ceramics and Superfine Microstructure, Shanghai Institute of Ceramics, Chinese Academy of Sciences, Shanghai 200050, China
[b] University of Chinese Academy of Sciences, 19 Yuquan Road, Beijing 100049, China
[c] School of Chemistry and Materials Science, Hangzhou Institute for Advanced Study, University of Chinese Academy of Sciences, 1 Sub-lane Xiangshan, Hangzhou 310024, China
[d] Tomsk Polytechnic University, 30 Lenin Ave, Tomsk 634050, Russia

ARTICLE INFO

Keywords:
MXenes
Post-processing
Atomic doping
Termination changing
Materials compounding
Two-dimensional materials

ABSTRACT

MXenes are a novel two-dimensional material family composed of transition metal carbides and carbonitrides that show promising performances in many applications. The intrinsic properties of MXenes are required to develop in different directions with the broadening applications. However, their properties are determined in the synthesis stage and are affected by various factors, such as precursor MAX phase, etchant, reaction time, and temperature. Since these parameters are difficult to control precisely, the targeted design of MXenes properties remains an open challenge. Herein, the post-processing modification of MXenes comes into play as a route to easily and efficiently tune and optimize their properties. This review critically discusses the research progress of MXenes' post-processing approaches to bridge the gap between theoretical predictions and properties observed experimentally. These strategies include atomic doping, functional group modification, and compounding with other materials, focusing on engineering electrical properties, mechanical properties, chemical stability, and the hydrophilic-hydrophobic nature of MXenes. We thus aim at providing a reference for customizing MXenes with targeted functionalities essential for future applications.

1. Introduction

Two-dimensional (2D) materials, with ultra-large specific surface area and a few atomic layers thick, result in systems with remarkable physical properties while providing a large density of active sites for chemical reactions in a very small volume. These characteristics of 2D materials are attracting extensive attention in various fields [1]. Following the discovery of numerous two-dimensional materials, such as grapheme [2], hexagonal boron nitride [3], and molybdenum disulphide [4], a large family of two-dimensional transition metal carbides or carbonitrides known as MXenes was first discovered in 2011 by Yury Gogotsi and his collaborators [5]. MXenes are produced by etching the A atomic layer in a layered precursor MAX phase ($M_{n+1}AX_n$), where M represents a transition metal, A is the element from groups IIIA or IVA, X is carbon and/or nitrogen, and n is from 1 to 4. Because of the MAX parent phase's diversity, over 100 possible structures for MXenes were predicted, and much more than 30 species with different elemental compositions and properties were successfully synthesized [6]. Among these new 2D materials, $Ti_3C_2T_x$ was discovered first and so it is the most widely studied so far [5,7–9].

As a critical part of MXenes' research, various synthesis strategies have been developed to meet the needs of different applications. The preparation procedure of MXenes commonly consists of etching and delaminating [10]. The etching process is mainly devoted to breaking the M−A metal bond in the precursor MAX phase. It can be divided into fluorine-containing acid etching [5,11,12], strong alkaline etching [13,14], halogen etching [15], electrochemical etching [16,17] and high-temperature etching [18]. Among them, fluorine-containing acid reagent or strong alkali is the most commonly employed to etch the A-layer. This process inevitably leads to the appearance of many dangling bonds on the surface of MXene nanosheets, which are converted into various terminations in an aqueous environment, such as -F, –OH, and -O. Meanwhile, more or fewer defects are introduced to the MXene nanosheets during the reaction, making this material easier to oxidize

* Corresponding authors.
E-mail addresses: wangranran@mail.sic.ac.cn (R. Wang), raul@tpu.ru (R.D. Rodriguez), jingsun@mail.sic.ac.cn (J. Sun).

https://doi.org/10.1016/j.cej.2021.131472
Received 14 April 2021; Received in revised form 15 July 2021; Accepted 18 July 2021
Available online 8 August 2021

and lose its original nature [19]. In the delamination stage, the multilayer MXenes peel off to form few- or single-layer lamellae under the action of mechanical vibration [5] or chemical intercalants [20,21] (positive ions, polar organic molecules, and organic alkaline macromolecules). However, the severe vibration during ultrasound will reduce the size of the MXene nanosheet, thus resulting in a significant loss in both electrical and mechanical properties. The employment of chemical intercalation avoids reducing MXenes' size to a certain extent, while it is difficult to completely remove these agents in subsequent processes, which also has a huge impact on the conductivity of MXenes film [22]. This makes the practical properties of MXenes quite different from theoretical values, thus limiting their applications in various fields, including energy storage [11,23–26], catalysis [27–29], electromagnetic shielding [30–35], flexible electronics [36–38], and chemical sensing [39,40].

Therefore, it is necessary to explore various post-processing modification approaches for MXenes combined with the theoretical calculation, catering to different application requirements. Herein, various approaches for the post-processing modification of MXenes are systematically summarized (Fig. 1), hoping to provide the theoretical basis and method support for the properties improvement of MXenes. Among these, the doping with non-metallic elements having weak electronegative promotes the transition of MXenes from semiconductor to metallic. Various post-treatment processes regulate the proportion of functional groups on the surface of MXenes. Introducing external functional groups endows MXenes with novel characteristics, and composition with polymer materials strengthens the binding among MXene nanosheets.

2. Theoretical and practical properties of MXenes

2.1. Electrical properties

According to density functional theory (DFT), the electrical properties of MXenes are related to the elemental composition and their surface termination [1,48]. In MXenes' family, carbides with surface termination always showed as semiconductors, while some carbonitrides with more electrons can promote the band structure change and transition to a metallic behaviour [1]. Monolayer MXenes with no termination are predicted to be metallic, while many MXenes terminated by O are expected to be semiconductive [5,49–51]. Specifically, when Yury Gogotsi and his team [5] firstly discovered MXenes, $Ti_3C_2(OH)_2$ and $Ti_3C_2F_2$ were theoretically predicted to have small bandgaps of 0.05 eV and 0.1 eV distinguished from metallic Ti_3C_2 (Fig. 2a). Although various synthesis routes of MXenes are continuously emerging, bare MXenes were not obtained so far. Instead, mixed terminations, including -F, -O, and –OH, randomly occupy the surface of MXenes and cause the localization of electronic states, changing their electrical and other properties. Therefore, from a theoretical perspective, it is possible to achieve targeted control of electrical properties by purposefully changing the element composition and/or surface termination of MXenes.

However, the actual electrical properties of MXene films are the macroscopic embodiment of multilayer stacked nanosheets so that the intercalation between layers also determines its electrical properties. For instance, the cations in reagents [52] (tetramethylammonium ion (TMA^+), ammonium ion (NH_4^+) and lithium-ion (Li^+)) and organic molecules [20] (dimethyl sulfoxide (DMSO) and isopropylamine) can all be intercalated into the layer spacing of MXenes, changing the electrical properties of MXene films. Consequently, the element composition, surface termination, and intercalation of MXene film can be controlled by post-processing modification, thus effectively realizing the targeted control of its electrical properties.

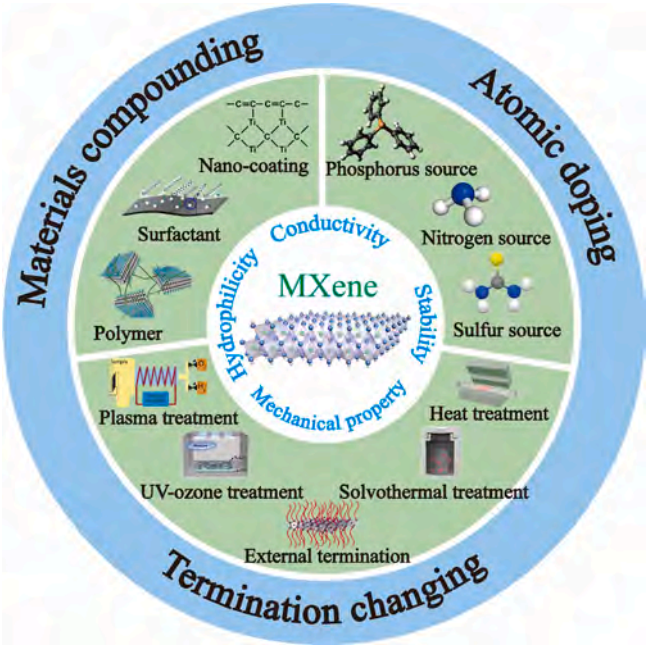

Fig. 1. Post-processing approaches and classification of MXenes. Partial insets were reprinted from literature.[22] Copyright 2020, The Royal Society of Chemistry.[41] Copyright 2019, Elsevier.[42] Copyright 2015, The Royal Society of Chemistry.[43] Copyright 2019, Wiley-VCH.[44] Copyright 2017, The Royal Society of Chemistry.[45] Copyright 2020, Elsevier.[46] Copyright 2018, The Royal Society of Chemistry.[47] Copyright 2017, Wiley-VCH.

2.2. Mechanical properties

Besides electrical properties, the mechanical properties of MXenes are attracting much attention in many applications. The mechanical properties of MXenes have already been investigated by Guo's team [53] by first-principles calculations. Their results indicate that the two-dimensional Ti_2C can endure large strains of 9.5% and 18% under biaxial and uniaxial tensions, respectively (Fig. 2b). After introducing -O terminations, the stretchable range of Ti_2CO_2 increased up to 20% and 28%, revealing the suppression effect of surface termination on the collapse of Ti_2C (Fig. 2c). Young's moduli of Ti_2C, Ti_3C_2, and Ti_4C_3 without termination were predicted using classical molecular dynamics yielding values of 597, 502, and 534 GPa, respectively [54]. However, the MXene films applied in the fabrication of devices are constructed by stacking multilayer nanosheets so that their mechanical properties are far lower than those for monolayer MXenes. For instance, the pure MXene films synthesized in Ling's work [12] possess Young's modulus of 3.52 GPa and a uniaxial tension of 1%, which is much lower than the prediction for monolayer nanosheets. The difference between the practical and theoretical mechanical properties of MXene films is mainly ascribed to the characteristics of nanosheets themselves and their weak interaction. The size, defect density, and incomplete edge of MXene nanosheets all affect their mechanical properties. Besides, the nanosheets combine with each other through van der Waals force, which lead to lower mechanical properties of macro films than that of MXene monolayer due to the weak interfacial interaction. To optimize the properties of MXene films, it is vital to enhance the interaction between monolayers. A very effective way to realize this is adding other binding agents.

In addition to the axial binding force, the mechanical properties perpendicular to the direction of the nanosheets are often reflected as their tribological properties. Due to the weak interaction and the easy-to-shear ability between nanosheets, MXenes exhibits comparable tribological properties with graphene [55]. Moreover, various MXenes materials and termination compositions endow them with adjustable tribological properties. Based on the previous research results, Anasori *et al.,* [56] predicted the tribological properties of different MXenes, thus providing guidance for future research work.

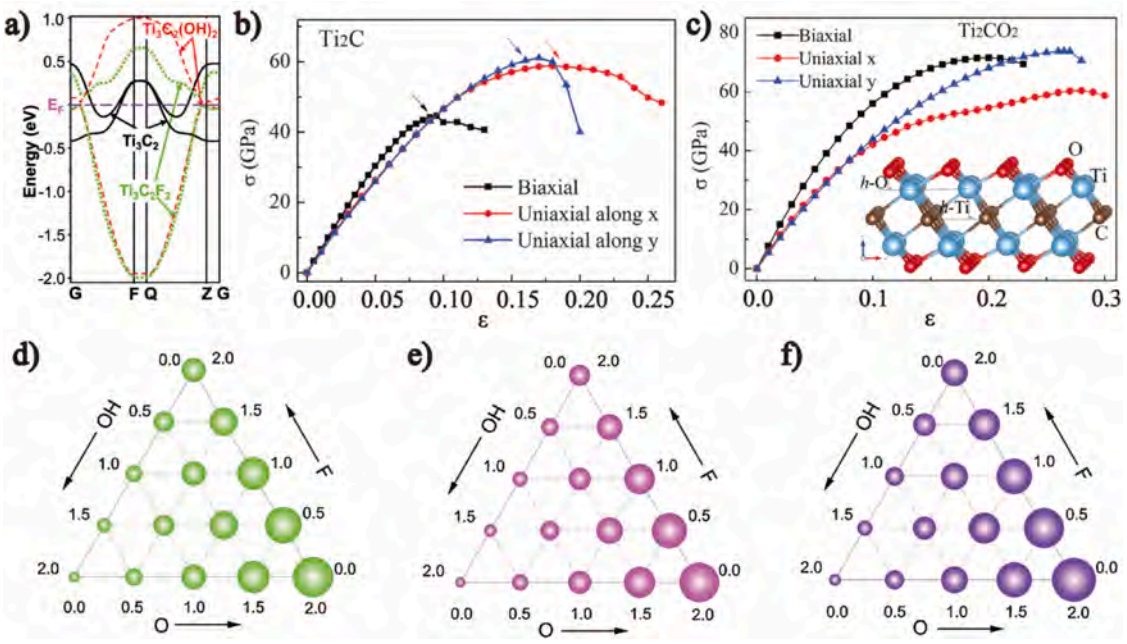

Fig. 2. (a) Calculated band structure of monolayer Ti_3C_2 with –OH and -F functional groups and without termination, corresponding to semiconductor and metal characteristics, respectively. Reprinted with permission.[5] Copyright 2011, Wiley-VCH. (b) Calculated stress–strain curves of Ti_2C without termination. These points marked by arrows are the strain at the beginning of instability. Reprinted with permission.[53] Copyright 2015, The Royal Society of Chemistry. (c) Calculated stress–strain curves of Ti_2C with -O functional group. The inset shows the atomic structure of Ti_2CO_2 with the functional group distribution in the most energetically favorable positions. Reprinted with permission.[53] Copyright 2015, The Royal Society of Chemistry. The relative stability of (d) Ti_3C_2, (e) Ti_2C. (f) Nb_4C_3 with mixed functional groups (-F, -O, and –OH). The larger the bubble size, the stronger the relative stability of MXenes. Reprinted with permission.[58]. Copyright 2018, American Chemical Society.

2.3. *Stability in the environment*

As a metastable phase, metal atoms distributed on the surface of MXenes deteriorate quickly under the action of oxygen, converting into oxides and losing their pristine structure [57]. To alleviate the loss of electrical and mechanical properties caused by oxidation, MXenes can be stored in oxygen-free or low-temperature environments, although at the cost of limited practical applications. Hu's work [58] clarified the ground-state stable structures of MXenes with mixed terminations (-O, -F, and –OH) by high-throughput computation screening, guiding the optimization of terminations. As shown in Fig. 2d-f, the stability of these MXenes (Ti_2C, Ti_3C_2, and Nb_4C_3) increases when the terminal group changes from –OH to -F to -O. Therefore, it is beneficial to enhance the anti-oxidation capability of MXenes by deliberately increasing the content of oxygen termination. Moreover, packaging MXene films by compounding with other materials also result in improved oxygen isolation preventing film deterioration [19,47,59,60]. Both the regulation of surface terminations and the compounding with other materials can be realized in the post-processing modification of MXenes.

Table 1
Summary of the post-processing modification for MXenes.

Types	Process method	Conductivity	Stability	Mechanical property	Hydrophilicity	Ref.
Atomic doping	NH_3; solvothermal	Increase	–	–	–	[61,62]
	$(C_6H_5)_3P$; heat treatment	Increase	–	–	–	[63]
	$(NH_2)_2CS$; heat treatment	Increase	–	–	–	[64]
Original termination changing	Vacuum; heat treatment	Increase	Increase	–	Decrease	[9]
	Ar; heat treatment	Increase	Increase	Increase	Decrease	[22,32,65]
	H_2; heat treatment	Increase	Decrease	–	–	[29]
	H_2 or O_2; plasma treatment	Increase (H_2); Decrease (O_2)	–	–	–	[44]
	Solvothermal in EtOH and DI	Increase	–	–	Increase	[41]
	UV-ozone treatment	Increase	–	–	–	[43]
External termination introducing	*p*-phenyl-SO_3H	Decrease	–	Decrease	–	[66]
	PFDTMS	–	Increase	–	Decrease	[67]
	PDMAEMA	–	–	–	Increase (low T/CO_2 uptake); Decrease (high T/CO_2 release)	[42]
Materials compounding	PEDOT: PSS; vacuum filtration	Decrease	–	Increase	–	[68]
	PVA; vacuum filtration	Decrease	Increase	Increase	Decrease	[12]
	NR; vacuum filtration	Decrease	Increase	Increase	Decrease	[45]
	CNF; vacuum filtration	Decrease	–	Increase	–	[69]
	Glucose; hydrothermal and heat treatment	–	Increase	–	Decrease	[47]
	CTAB; regulating pH of aqueous phase	–	–	–	Increase (acidic); Decrease (alkaline)	[46]

3. The post-processing modification approach of MXenes

This section summarizes a series of research progress concerning the post-processing modification of MXenes divided into two categories: chemical modification (atomic doping and termination changing) and physical composites (materials compounding). The specific process method, conductivity changes, stability, mechanical properties, and hydrophilicity of MXenes are summarized in Table 1.

3.1. Mxenes modified by atomic doping

According to previous calculation results, doping other atoms with more electrons, such as nitrogen, sulfur, phosphorus, and other elements, into the carbide MXenes can change their band structure, thus improving the electrical conductivity [1]. Among these, nitrogen doping carbide MXenes was widely studied to promote the transition from semiconducting to metallic [62]. Additionally, several carbides were discovered earlier and are now better understood in MXenes' family. When the doping ratio is large enough, the Mo_2CT_x carbide MXene can be transformed entirely into 2D nitrides *via* ammoniation at 600 °C, which provides an unconventional route for the synthesis of nitride-based MXenes [61].

Yang *et al.,* [62] presented a process based on nitrogen doping by solvothermal treatment, where urea saturated alcohol solution or monoethanolamine provided a liquid nitrogen source for delamination of Ti_3C_2 (d-Ti_3C_2). The deconvolution of N 1 s peaks in the XPS spectra from UN-Ti_3C_2(urea saturated alcohol solution) and MN-Ti_3C_2 (monoethanolamine) was used to determine whether nitrogen atoms were successfully incorporated into Ti_3C_2. It is noteworthy that the existence of N-5 effectively improves the conductivity of Ti_3C_2 nanosheets because of their excellent electron donor character. Similarly, N-6 conjugates a pair of electrons and π-conjugated rings, showing electron donor character in UN-Ti_3C_2. The experimental results confirm this point, in which the resistance of MN-Ti_3C_2, UN-Ti_3C_2, and d-Ti_3C_2 are 3.1, 3.3, and 3.4 Ω, respectively.

Another commonly used nitrogen doping process is a heat treatment in an ammonia atmosphere, through which the carbide MXenes can be converted entirely into nitrides by adjusting the treatment temperature. In Urbankowski's work [61], Mo_2C and V_2C, as two carbide MXenes precursors, were transformed into Mo_2N and V_2N phases by ammoniation (Fig. 3a). After heat treatment at 600 °C, Mo_2N retained the layered MXene structure, while V_2N turned into a layered structure composed of trigonal V_2N and cubic V_2N, indicating the selectivity of MXenes precursors in this unconventional synthesis approach. Additionally, lower heat treatment temperature resulted in partial nitrogen doping rather than complete nitridation. Element analysis of the sample under different processing conditions and the XPS results confirmed the bonding between nitrogen and metal atoms, while the C-metal bonding was suppressed or weakened (Fig. 3b). During the subsequent resistance measurements, the pristine Mo_2CT_x films were treated in an inert atmosphere under the same conditions to eliminate defects introduced by heat treatment. It was found that the resistivity of the treated Mo_2CT_x film was still higher than that of Mo_2NT_x film by one order of magnitude.

The conductivity of MXenes can be improved by doping not only with nitrogen but also with other elements with electronic donor character, including phosphorus [63] and sulphur [64]. To get P-doped V_2C with controllable composition, triphenylphosphine (TPP) as a phosphorus source was mixed with MXene, and then the mixture was heat-treated under the protection of argon at different temperatures (300–500 °C) (Fig. 3c). When the heat treatment temperatures increased gradually, the doping degree of phosphorus changed. In accordance with the phosphorous increase deduced from XPS spectra, the conductivity of V_2CT_x also increased with the phosphorus content.

In another work [64], Li and his team investigated sulfur doping of multilayer $Ti_3C_2T_x$, in which the hydrogen sulfide produced by the decomposition of thiourea during heat treatment was used as a sulfur source. Meanwhile, the different heat treatment temperatures were employed to control the sulfur concentrations in pristine $Ti_3C_2T_x$. The XPS results prove that sulfur occupied the position of partial carbon atoms in $Ti_3C_2T_x$. In further experiments, the higher the sulfur doping level, the smaller the sample's electrical resistance, which is identical to the effect of doping with other electronic donor elements.

These three elements are non-metal atoms with low-electronegativity (nitrogen 3.04, sulfur 2.58, and phosphorus 2.19) [63] that can provide electrons and change the MXenes band structure. Therefore, non-metallic doping with low electronegativity into carbide

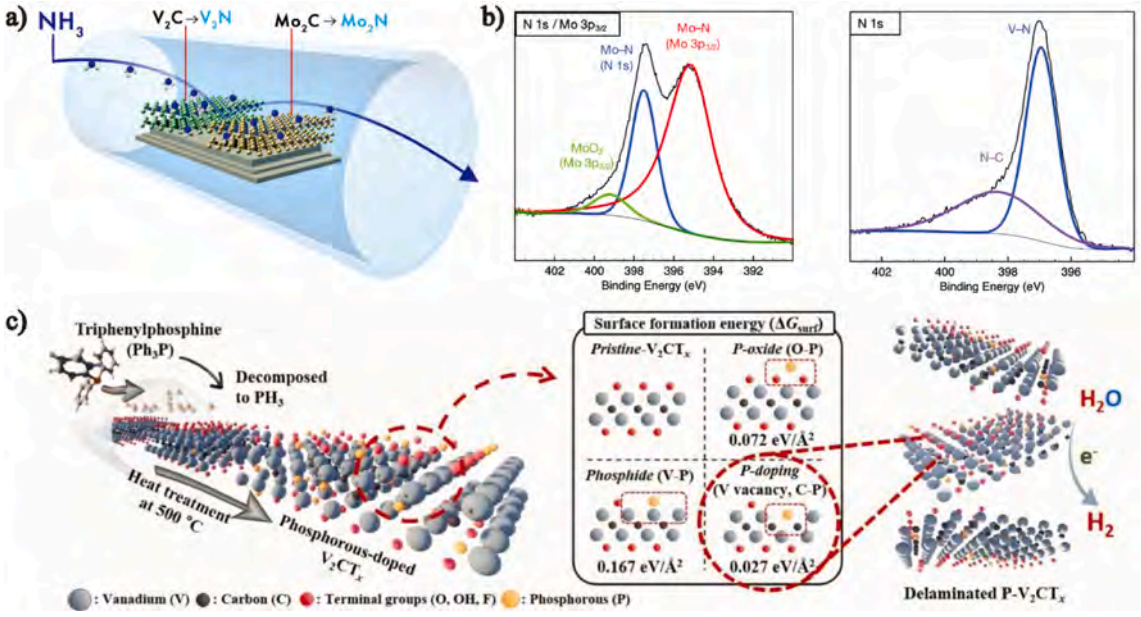

Fig. 3. (a) The synthesis process from transition metal carbides (Mo_2CT_x and V_2CT_x) to nitride MXenes. Reprinted with permission.[61] Copyright 2017, The Royal Society of Chemistry. (b) The N 1 s XPS spectra for Mo_2N and V_2N synthesized by ammoniation of carbide MXenes. Reprinted with permission.[61] Copyright 2017, The Royal Society of Chemistry. (c) Schematic illustration of phosphorus doping for V_2CT_x by heat treatment with $P(Ph)_3$ (TPP) and their possible atomic structure determined from surface formation energy calculations. Reprinted with permission.[63] Copyright 2019, Wiley-VCH.

MXenes can promote their transition from semiconductor to metallicity. In addition, atomic doping further expands the interlayer spacing and increases the specific surface area of MXenes, and enable them to prepare electrodes with high specific capacity for energy storage devices and electrodes with high activities for electrocatalytic reactions.

3.2. Mxenes modified by terminations regulation

Besides doping MXenes with other elements, the abundant terminations connected to their surface provide more extensive possibilities for post-processing modification. Many MXenes' properties are determined by the mixed terminations (-F, –OH, and -O) on their surface introduced during the synthesis process. Moreover, the introduction of external functional groups endows MXenes with unconventional hydrophobicity [67], positive surface potential [70], and high sensitivity to their environment [42]. This section summarizes the post-processing modification approaches used mainly for changing the functional groups on the surface of MXenes.

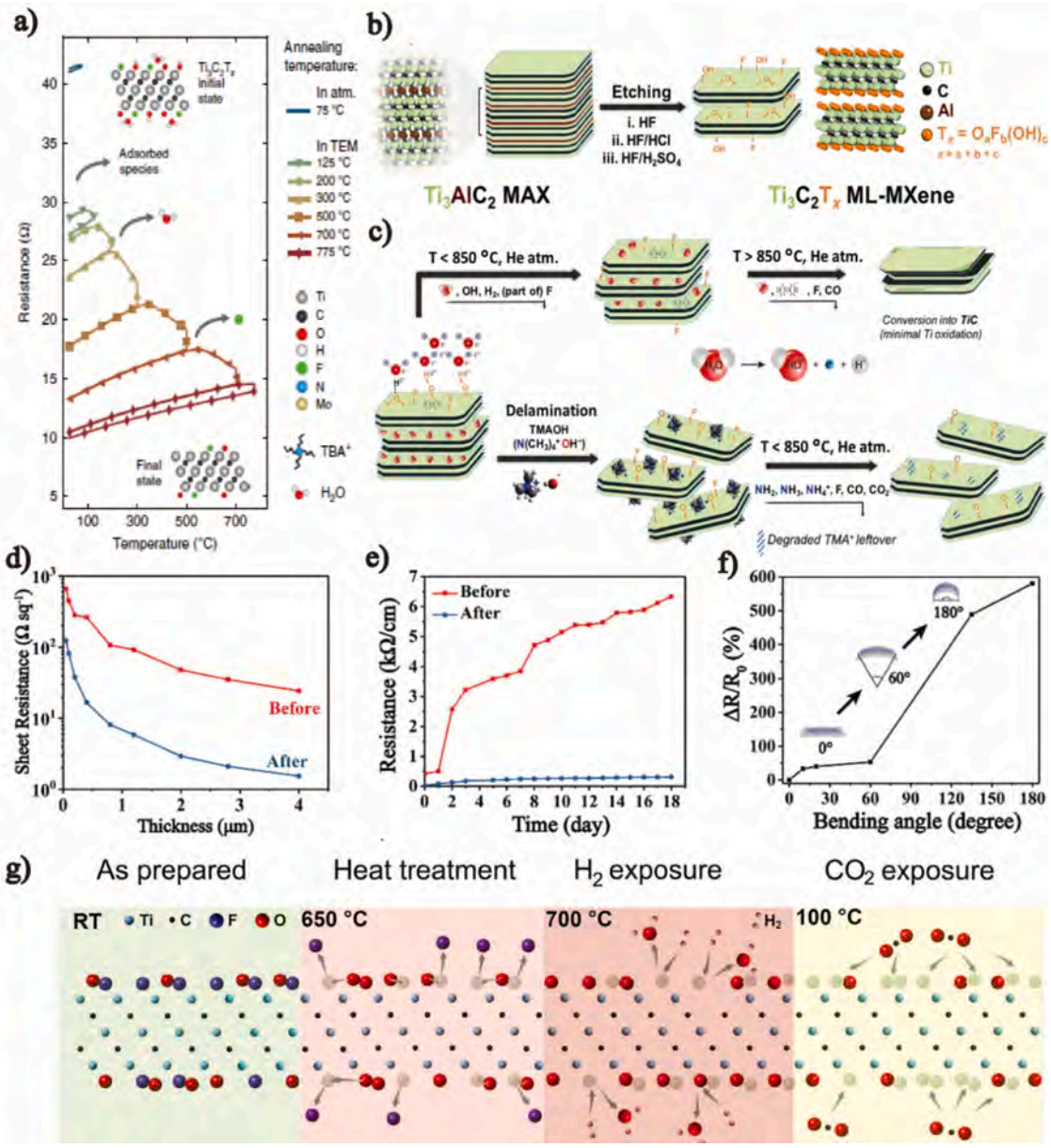

Fig. 4. (a) The effect of in-situ vacuum annealing temperature on $Ti_3C_2T_x$ resistance. The curves with different colors correspond to different vacuum annealing processes, including heating and cooling stages. The atomic structures of $Ti_3C_2T_x$ in the initial and final states are shown as insets. Reprinted with permission.[9] Copyright 2019, Springer Nature Publishing. (b) Multilayer $Ti_3C_2T_x$ MXene synthesized with different etchants such as HF, HF/HCl, or HF/H_2SO_4. Reprinted with permission.[65] Copyright 2019, American Chemical Society. (c) The variation of $Ti_3C_2T_x$ treated by different approaches during heat treatment. MXenes undergo partial oxidation and phase transition in a He environment when the temperature exceeds 850 °C. The oxidation is caused by hydroxyl radicals (HO·) and superoxide anions (O_2^-) produced during heat treatment. Reprinted with permission.[65] Copyright 2019, American Chemical Society. (d) Effect of heat treatment on the conductivity of $Ti_3C_2T_x$ films with different thicknesses. Reprinted with permission.[22] Copyright 2020, The Royal Society of Chemistry. (e) Stability of $Ti_3C_2T_x$ films before and after heat treatment in an atmospheric environment. Reprinted with permission.[22] Copyright 2020, The Royal Society of Chemistry. (f) Response of heat-treated film to bending. Reprinted with permission.[22] Copyright 2020, The Royal Society of Chemistry. (g) Schematic illustration of surface termination changes distributed on $Ti_3C_2T_x$ nanosheets under different treatment stages and environmental atmosphere. Reprinted with permission.[29] Copyright 2019, Wiley-VCH.

3.2.1. No external functional groups introduced

For most of the synthesis routes, the functional group on the surface of MXenes is mainly composed of -F, -O, and –OH with different proportions. Without introducing external functional groups, post-processing modification is carried out to change the content of these pristine functional groups, thus mainly focusing on the control of MXenes' intrinsic properties.

3.2.1.1. Termination changing by heat treatment. As the most commonly used method to change the surface termination of MXenes, heat treatment is reviewed as a solo section. Different atmospheres and additives can make the surface termination of MXenes develop in entirely different directions. Previous studies showed that if Ti_2CT_x was annealed in air, it would turn into titanium oxide (TiO_2) nanoparticles and graphite carbon [71]. Therefore, to maintain the atomic and chemical structure of MXenes, the heat treatment must be performed in vacuum or an inert or reductive atmosphere. The effect of vacuum and the inert atmosphere is similar, preventing the reaction between MXenes and oxygen. In Hart's work [9], the in-situ heat treatment of $Ti_3C_2T_x$ in vacuum was investigated, and the internal relationship between conductivity and the de-functionalization of the sample's surface was revealed using electrical biasing and spectroscopic analysis. Fig. 4a shows the real-time resistance curve of $Ti_3C_2T_x$ at different temperatures, where the three stages of resistance reduction are due to the separation of adsorbed species, the water molecules desorption, and the fluorine content reduction. DFT calculation results suggested that the –OH in mixed terminations should be the first to be removed during heat treatment, but its signal could not be detected by thermogravimetry mass spectrometry (TG-MS) because of the covering of water molecules. Additionally, the de-functionalization of -F with high electronegativity can change the band structure of MXenes and improve their electrical conductivity.

Seredych's work [65] explored the impact on MXenes processed at a higher temperature (1500 °C) in helium (He) atmosphere through TG-MS analysis. The multilayer $Ti_3C_2T_x$ etched by HF and the delaminated $Ti_3C_2T_x$ treated by TMAOH were characterized with results shown in Fig. 4b, c. The water signal for multilayer $Ti_3C_2T_x$ synthesized by high concentration HF changed dramatically at 200 and 320 °C, respectively. The former mainly comes from the release of intercalated water molecules between nanosheets (weak water–water interaction), while the latter is related to the water molecules bound to the –OH termination of $Ti_3C_2T_x$ (strong water–surface interaction) [72,73]. If post-processing involves the –OH termination and water molecules, the pristine good hydrophilicity of MXenes will also be affected. In the sample intercalated by TMAOH, there is a significant change in the signal of $NH_2/NH_3/NH_4^+$, which is responsible for the decomposition of the cationic group (TMA^+). Besides removing terminal groups, high-temperature treatment can also cause the phase transition of MXene, resulting in the transformation of crystal structure and material properties. When the phase transition temperature (800 °C) was reached, the pristine chemical structure of $Ti_3C_2T_x$ was destroyed and transformed into cubic titanium carbide (TiC) with the release of carbon monoxide (CO), while the excellent conductivity and other properties of the original material also disappeared. The existence of a phase transition temperature for MXenes also clarifies the upper limit of temperature in thermal post-processing.

The properties variation of $Ti_3C_2T_x$ obtained by TMAOH intercalation during low-temperature heat treatment was mainly studied in Tang's work [22]. The heating process to 300 °C and holding temperature can remove the water molecules and residual intercalation agent from $Ti_3C_2T_x$, leading to the film structure densification. Besides, the heat treatment process reduces the content of -F terminal group and completely removes the TMA^+ cationic group. For these reasons, the sheet resistance of $Ti_3C_2T_x$ film decreases about 15 times before and after treatment (Fig. 4d). In addition to conductivity, the stability in ambient conditions and mechanical properties of $Ti_3C_2T_x$ film were also improved significantly as shown in Fig. 4e, f.

Although the spacing between MXene nanosheets (calculated from the position of 002 peak) decreases during annealing in an inert atmosphere, slit pores with size distribution ranging from tens of nanometers to micrometers appear in the whole film structure, which was reported in Iqbal's work [32]. As shown in the cross-section TEM images of Ti_3CNT_x film, the pore size and pore volume of the film increase with annealing temperature, which is attributed to the removal of water intercalation and the desorption of surface molecules. Besides temperature, the porosity of MXene film is positively correlated with their thickness. This is because many gaseous substances produced in the heating process are difficult to escape from the compact layered structure, thus forming larger pores in the thicker film. The monotonically increase in conductivity of $Ti_3C_2T_x$ film is mainly due to the decreased spacing between nanosheets (calculated from the position of 002 peak, maximum: 5225 S cm^{-1}), which promotes the interlayer electron conduction. As for Ti_3CNT_x (maximum: 2475 S cm^{-1}), the opposite phenomenon of conductivity variation at 350 °C is mainly caused by the increase of pore volume.

In contrast to vacuum and inert gas, the employment of reductive atmosphere and alkaline additives in heat treatment mainly affects the proportion of O-containing terminations (-O and –OH) on the MXenes surface. Persson and his team [29] heat-treated $Ti_3C_2T_x$, whose surface termination was mainly composed of -F and -O, in environmental transmission electron microscopy. The sample was first heated to 650 °C in vacuum to remove the -F termination. Subsequently, the hydrogen atmosphere introduced at 700 °C reacted with the -O surface termination, thus resulting in the $Ti_3C_2T_x$ with local termination-free (Fig. 4g). Based on previous DFT calculations, it is reasonable to speculate that the $Ti_3C_2T_x$ with local termination-free should exhibit higher metallicity rather than a semiconducting behavior. However, it is not stable and needs to be passivated by other terminations, which in their paper corresponds to carbon dioxide adsorption.

In another work [74], the -O termination content was increased by adding alkaline additives in the process of heat treatment. First, the $Ti_3C_2T_x$ (E-$Ti_3C_2T_x$) intercalated by dimethyl sulfoxide (DMSO) was dispersed in potassium hydroxide (KOH) aqueous solution so that a large number of -F terminations were replaced by –OH. The oxygen functionalized Ti_3C_2 (E-$Ti_3C_2O_x$) was transformed from $Ti_3C_2(OH)_x$ (E-$Ti_3C_2(OH)_x$) through heat treatment at 450 °C in argon atmosphere. Although that work did not focus on the influence of terminal groups on the conductivity, hydrophilicity, or stability of MXene nanosheets, it is easy to draw conclusions based on other theoretical studies. The -F termination substitution is beneficial to the improvement of MXenes conductivity, and the existence of a large number of –OH terminations can enhance the nanosheet hydrophilicity further. According to DFT predictions, the oxygen functionalized Ti_3C_2 ($Ti_3C_2O_x$) should be more stable than those with other terminations.

During the heat treatment process, the surface functional group evolusions of MXenes are mainly determined by temperature and atmosphere. With the increase of treatment temperature, the terminations distributed on MXene surface decrease in the order of - OH, - F, - O, which improved their conductivity and environmental stability. Therefore, this treatment is often employed for improving the conductivity of MXenes-based transparent conductive films. Moreover, the slit pores appeared in thick MXene films after heat treatment can significantly improve their electromagnetic shielding performance. However, the existence of MXenes phase transition point determines the upper limit of heat treatment. Beyond this point, the original crystal structures and material properties of MXenes will change. For the environmental atmosphere, both vacuum and inert gas are able to prevent the oxidation of MXenes. The reductive atmosphere is special, which can react with the -O termination at high temperature to form MXenes with local termination-free.

3.2.1.2. Termination change by other processes. Besides the common heat treatment process, many other post-processing modification approaches are devoted to changing the surface termination of MXenes. For instance, plasma treatment [44] in different atmospheres could achieve a repeatable resistivity switching in a $Ti_3C_2T_x$ film from 5.6 μΩ (oxidized state) to 4.6 μΩ (reduced state). The experimental setup layout of plasma treatment in Fig. 5a shows separate inlets for introducing hydrogen and oxygen into the chamber. The $Ti_3C_2T_x$ film was plasma treated under alternate hydrogen and oxygen atmospheres while the resistivity change was monitored in real-time (Fig. 5b). In the hydrogen plasma treatment stage, the $Ti_3C_2T_x$ film resistivity decreased dramatically with a variation reaching the peak value of ~ 18% at 11 min. The $Ti_3C_2T_x$ film resistivity gradually increased and returned to the initial level after switching to oxygen. This reversible transformation also appeared in subsequent plasma treatment cycles. The intensity of TiO_2/$TiO_{2-x}F_x$ peak and O-containing terminations all increase significantly after the oxygen plasma treatment. Although the second hydrogen plasma could not make the sample return to the initial state, it also reduced partial oxides and O-containing terminations in $Ti_3C_2T_x$ film. Therefore, the plasma treatment process can control the O-containing terminations of MXenes to a certain degree, thus enabling a reversible transformation of their conductivity.

Besides, solvothermal treatment is also an effective way to modify the surface termination of MXenes. Ethanol (Et) and deionized water (DI) were used as low toxic solvents and participated in the solvothermal treatment of Nb_2CT_x, during which the layer spacing and surface termination were easily changed (Fig. 5c) [41]. The FTIR and XPS spectra were employed to analyze the variation of surface termination composition. By employing solvothermal treatment with ethanol or deionized water, the -F termination can be replaced by –OH, and the proportion of other O-containing functional groups on MXenes surface is also significantly increased, helping to narrow the separation between valence and conduction bands.

Meanwhile, the surface Ti-O bond of MXenes can also be induced by UV-ozone treatment [43], which was investigated in Yang's work (Fig. 5d). The surface chemical state of $Ti_3C_2T_x$ films treated with UV-ozone for different times was characterized by XPS. As shown in Fig. 5e, the doublet centered at 458.3 and 464.3 eV in Ti 2p spectra correspond to Ti-O bond (green), which came entirely from $Ti_3C_2T_x$. The doublet intensity increased with the extension of UV-ozone treatment time and reached the maximum value at 30 min, implying an increasing content of O-containing terminations. The narrowing of the MXene bandgap is attributed to the extra O-containing terminations that occupied some active sites initially linked to the -F termination.

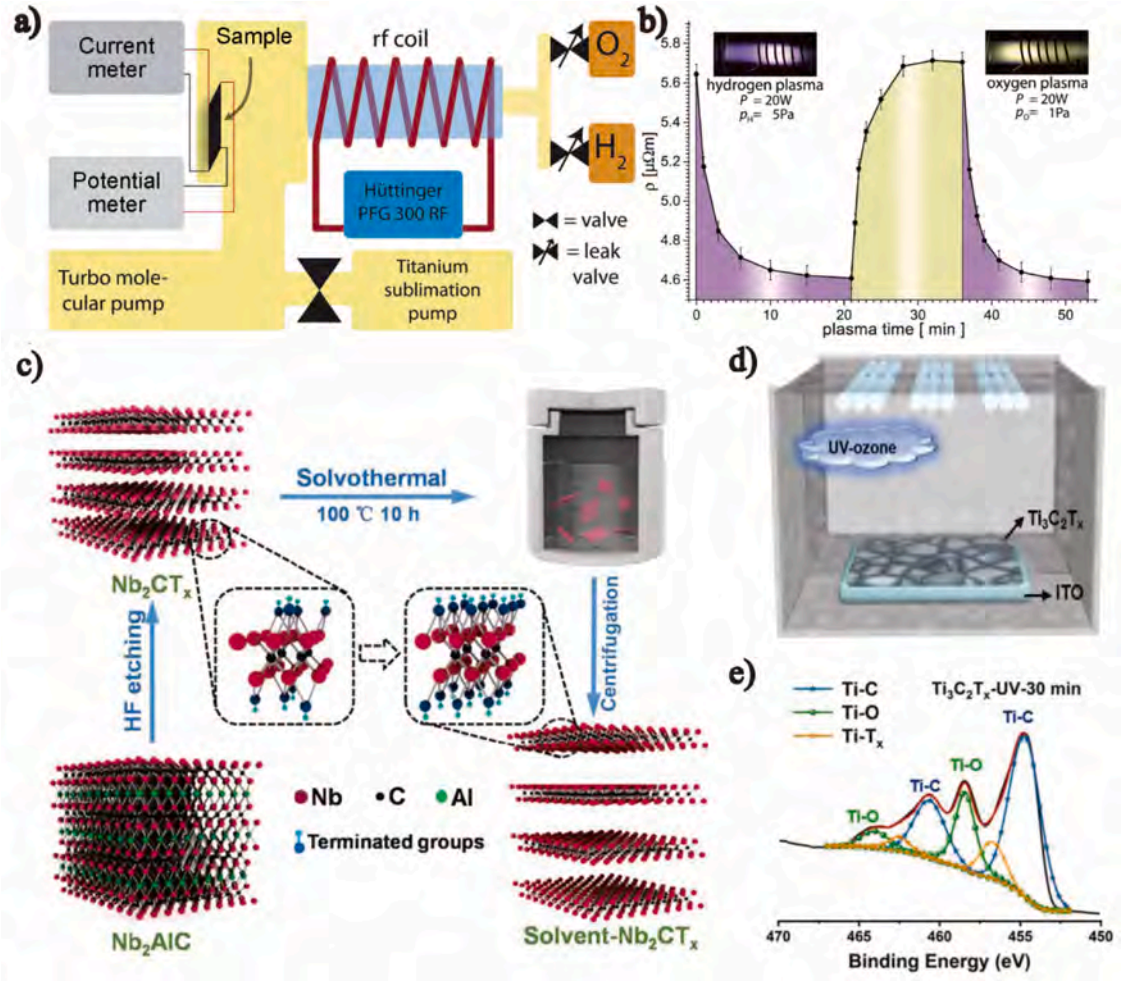

Fig. 5. (a) Schematic illustration of plasma equipment. The yellow area represents the vacuum environment, and the light blue area is used to excite the plasma with the RF coil. Adapted with permission.[44] Copyright 2017, The Royal Society of Chemistry. (b) The change of $Ti_3C_2T_x$ resistivity in the process of plasma treatment. Each resistivity value is obtained by fitting the slope of a bipolar *IV*-curve to at least 10 data points. Reprinted with permission.[44] Copyright 2017, The Royal Society of Chemistry. (c) Schematic illustration of Nb_2CT_x synthesis and subsequent solvothermal treatment. Reprinted with permission.[41] Copyright 2019, Elsevier. (d) Schematic illustration of UV-ozone treatment on $Ti_3C_2T_x$. Reprinted with permission.[43] Copyright 2019, Wiley-VCH. (e) The Ti 2p XPS spectra of $Ti_3C_2T_x$ film after being UV-ozone treated for 30 min. Reprinted with permission.[43] Copyright 2019, Wiley-VCH.

3.2.2. Introduction of external functional groups

The MXenes surface is inevitably terminated by various functional groups in the synthesis process, which affect MXenes' properties, providing lots of active sites for introducing external functional groups. Grafting other functional groups to the surface of MXenes by chemical reactions will undoubtedly endow them with new extra features.

Although multilayer MXenes can be delaminated by ultrasonic vibration, they agglomerate again after some time, greatly affecting their stability in aqueous dispersions [66]. To solve this problem, phenylsulfonic groups with negatively charged units were anchored on the surface of Ti_3C_2, promoting their delamination effect and keeping good dispersion in deionized water. As shown in Fig. 6a, the first intercalation of Na^+ initially expanded the spacing between Ti_3C_2 layers and provided enough space for the accommodation of aryl diazonium salts. Spacing between Ti_3C_2 layers was further enlarged with the successful introduction of phenyl-SO_3H groups, achieving good dispersion of the Ti_3C_2 nanosheets in deionized water. The FTIR characterization results in Fig. 6b show that the sample after modification (MXene-SO_3H) exhibits five new characteristic vibrations. The sample was further characterized by XPS with the high-resolution S 2p XPS spectrum shown in Fig. 6c. These two analysis results combined demonstrate the successful grafting of phenylsulfonic acid groups on the surface of Ti_3C_2. Moreover, there is no peak related to nitrogen (N) in the whole XPS spectrum, which implies that the diazonium group in the aryl diazonium salt absorbed the electrons of MXene and converted them into nitrogen (N_2). Meanwhile, the aryl radical is connected to the MXenes surface. The larger space volume of phenylsulfonic acid groups and the higher negative potential (-30.6 mV) of modified Ti_3C_2 nanosheets effectively prevented their agglomeration, thus endowing them with good dispersion in deionized water.

Besides, the chemical grafting of [3-(2-aminoethylamino)-propyl] trimethoxysilane (AEAPTMS) was carried out to realize the amine functionalization of Ti_3C_2 surface and change its surface potential in Riazi's study [70]. These AEAPTMS molecules were connected to the $Ti_2C_2T_x$ surface by the covalent bonding between silanol group ends and hydroxyl (Fig. 6d) or the electrostatic interaction of the amine group ends. It should be noted that the temperature, pH, water/ethanol ratio, and the type of aminosilane coupling agent are all critical conditions that affect the grafting effect of AEAPTMS molecule. The methoxy groups in the silane coupling agent were converted into hydroxyl groups after hydrolysis, and the resulting silanol groups were covalently bonded to the hydroxyl groups on the $Ti_3C_2T_x$ surface. Due to the presence of free amino groups, the surface potential of modified $Ti_3C_2T_x$ is always more than + 20 mV in the pH range of 2.5–10 (Fig. 6e), which is entirely different from that of pristine samples (negative charge). Therefore, this grafting of AEAPTMS molecule can make the self-assembly of MXenes possible (between MXene nanosheet with a positive charge and negative charge, Fig. 6f), while opening new possibilities for subsequent reactions.

Introducing external functional groups can also change the hydrophilic-hydrophobic character of MXenes or make them sensitive to environmental conditions. Zhao and his team [67] successfully prepared a kind of hydrophobic MXene film modified by trimethoxy (1H,1H,2H,2H-perfluorodecyl)silane (PFDTMS). The molecular structure of PFDTMS is given in Fig. 7a, which was firstly hydrolyzed to siloxane and further polycondensated to form oligomers. Subsequently, the hydrophilic group in oligomers reacted with the –OH termination on the Ti_3C_2 surface to form numerous stable ether bonds. With the coverage of -CF_3 groups, the Ti_3C_2 films after modification showed a hydrophobic character. The FTIR spectra of Ti_3C_2 before and after modification are compared, where the –OH peak centered at 3437 cm^{-1} appeared in the pristine sample and disappeared in the modified sample. As shown in Fig. 7d, the contact angle of Ti_3C_2 film increased from 38.8° to 102.0° after PFDTMS modification.

In another study published by Chen's team [42], poly(2-(dimethylamino)ethyl methacrylate) (PDMAEMA) brushes bound to the V_2C surface through self-initiated photografting and photopolymerization (SIPGP) (Fig. 7c). The dual response of PDMAEMA for CO_2 and temperature endows this hybrid material system with a sensibility to external stimuli. The reversible hydrophilic-hydrophobic transition of V_2C@PDMAEMA hybrids system affected their dispersibility in deionized water, thus controlling the conductivity of the aqueous solution. As a thermosensitive polymer, the PDMAEMA chain was hydrophilic and swelled at room temperature, while it became hydrophobic and shrank above the lower critical solution temperature (LCST), leading to good dispersion or quick accumulation for this hybrid material system at different temperatures. Moreover, the tertiary amino group in PDMAEMA can be protonated by CO_2 to form charged ammonium

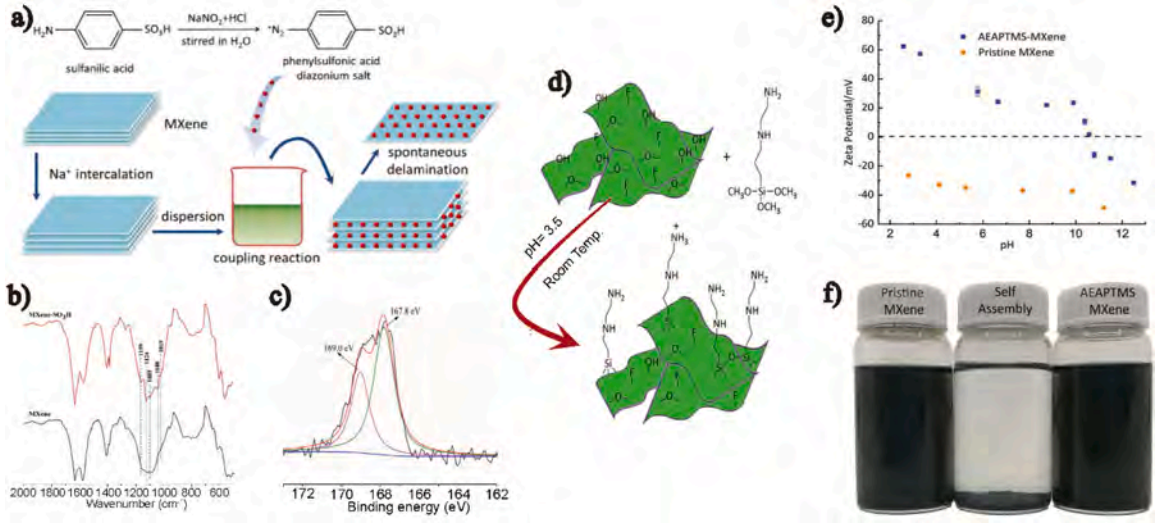

Fig. 6. (a) Schematic illustration for surface modification of multilayer $Ti_3C_2T_x$ with aryl diazonium salts. Reprinted with permission.[66] Copyright 2016, Elsevier. (b) The FTIR spectra of Ti_3C_2 before and after modified by aryl diazonium salts. Reprinted with permission. [66] Copyright 2016, Elsevier. (c) The S 2p XPS spectrum of Ti_3C_2 after modification. Reprinted with permission.[66] Copyright 2016, Elsevier. (d) Schematic illustration for surface modification of $Ti_3C_2T_x$ with [3-(2-aminoethylamino)propyl]trimethoxysilane (AEAPTMS) coupling agent. Reprinted with permission.[70] Copyright 2020, Wiley-VCH. (e) Surface charge of $Ti_3C_2T_x$ before and after AEAPTMS modification at different pH values. Reprinted with permission.[70] Copyright 2020, Wiley-VCH. (f) Self-assembly of $Ti_3C_2T_x$ formed by mixing MXene with opposite surface charge. Reprinted with permission.[70] Copyright 2020, Wiley-VCH.

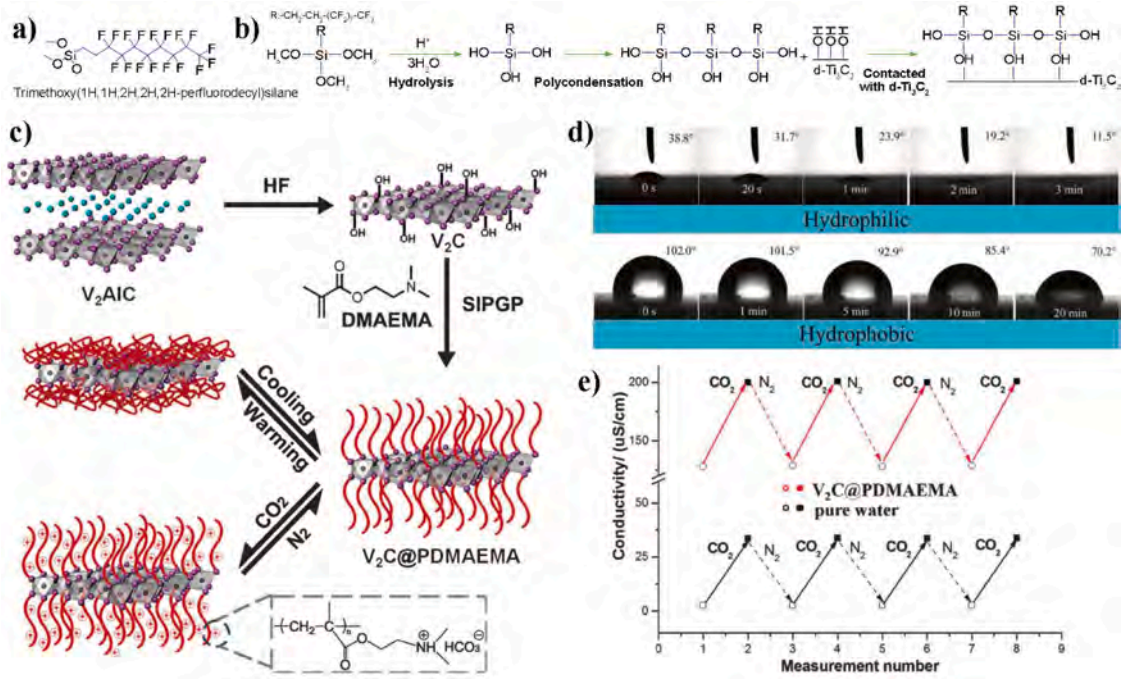

Fig. 7. (a) The molecular structure of PFDTMS. Reprinted with permission.[67] Copyright 2018, The Royal Society of Chemistry. (b) Schematic illustration of grafting PFDTMS onto Ti_3C_2 surface. Reprinted with permission.[67] Copyright 2018, The Royal Society of Chemistry. (c) Schematic illustration of grafting PDMAEMA onto V_2C surface (C atom: gray white, V atom: purple, Al atom: blue). Reprinted with permission.[42] Copyright 2015, The Royal Society of Chemistry. (d) Time course contact angles of Ti_3C_2 film before and after modification. Reprinted with permission.[67] Copyright 2018, The Royal Society of Chemistry. (e) Conductivity changes of V_2C@PDMAEMA suspension measured at 25 °C during repeated CO_2 uptake-release process. The concentration of aqueous suspension is 3.0 mg mL^{-1}. The average conductivity value was calculated from three measurements. Reprinted with permission.[42] Copyright 2015, The Royal Society of Chemistry.

bicarbonate, thus controlling the conductivity of V_2C@PDMAEMA suspension by adsorption or removal of CO_2 (Fig. 7e).

The introduction of external functional groups endows MXenes with broader functional diversity, thus realizing the customization of MXenes to fit different applications. Specifically, the MXene films experienced hydrophobic transition have better salt-blocking property and environmental stability, which is expected to be employed in solar seawater purification. MXenes grafted with smart materials can be used to sense various environmental factors such as temperature and gas content. Furthermore, the availability of active sites on external functional groups makes the fabrication of MXenes based composites, adsorbents, and drug carriers possible.

3.3. Mxenes modified by materials compounding

Among all post-processing modification approaches, the simplest and most effective way is to compound other materials into MXenes matrices. The properties of such hybrid systems are significantly changed by hydrogen bonding, ion binding, and other interactions formed between diverse components. This section summarizes the research progress of MXenes in changing their mechanical properties, stability, and hydrophilicity by compounding with various materials.

3.3.1. Compounding for mechanical property enhancement

Although monolayer MXenes have a large theoretical strain range and Young's modulus, the MXene films are all made by stacked multilayer nanosheets, which leads to the significant difference in mechanical properties between theoretical and actual values. With external loadings applied to the MXene film, cracks often appear between nanosheets rather than inside them, thus it is necessary to enhance the binding force among nanosheets. Therefore, many materials, such as polyvinyl alcohol (PVA) [12], natural rubber (NR) [45,75], cellulose nanofibers (CNFs) [69,76–78], poly(3,4-ethylenedioxythiophene)/poly(styrenesulfonate) (PEDOT/PSS)[68,79], and polyaniline (PANI) [80], are compounded into MXenes to form a strong interaction, which significantly improves the mechanical properties of this hybrid system.

Inspired by the nacre-like "brick-and-mortar" structure, the film composite made from $Ti_3C_2T_x$ and PEDOT:PSS was assembled *via* vacuum filtration in Liu's work [68]. Based on this bionic structure, the mechanical interlock at the nanometer level was realized between $Ti_3C_2T_x$ and PEDOT: PSS, thus greatly improving the mechanical properties of the composite film. The composite film presents the highest tensile strength (30.18 MPa) when the $Ti_3C_2T_x$/PEDOT:PSS ratio is 3: 1, which is 5.4 times higher than pure $Ti_3C_2T_x$ film (5.62 MPa). In another study [12], electrically neutral polyvinyl alcohol (PVA) was compounded with $Ti_3C_2T_x$, producing a composite film with good flexibility. Their stress–strain curves more intuitively describe the mechanical properties of $Ti_3C_2T_x$/PVA composite films with different MXene content, in which the tensile strength increases by 34% with the addition of 10 wt% PVA into pure $Ti_3C_2T_x$.

Moreover, natural rubber (NR), mainly composed of *cis*-1,4-polyisoprene units [45], was also used as an additive to obtain a MXene-based composite film with good mechanical properties by vacuum filtration (Fig. 8a-d). The downshift of (0 0 2) peak in XRD patterns indicates the increased spacing between MXene nanosheets after the intercalation of NR. In folding endurance tests, the maximum number of folding cycles for pure MXene films was 119, while the composite film with the addition of 10% NR resisted up to 327 folding cycles. Cao and his team [69] mixed one-dimensional cellulose nanofiber (CNF) and two-dimensional $Ti_3C_2T_x$ nanosheet to prepare a composite film by vacuum filtration (Fig. 8e-h). There are abundant terminations (such as -F, -O, and –OH) on the surface of $Ti_3C_2T_x$ after wet chemical etching, while the CNFs extracted from microcrystalline cellulose also have many active hydroxyl sites, resulting in the formation of a large number of hydrogen bonds at the interface of two components. Moreover, the anisotropic interconnection networks constructed by one-dimensional CNFs and two-dimensional $Ti_3C_2T_x$ nanosheets also benefit crack deflection, which eventually led to a "zigzag" crack path at the fracture

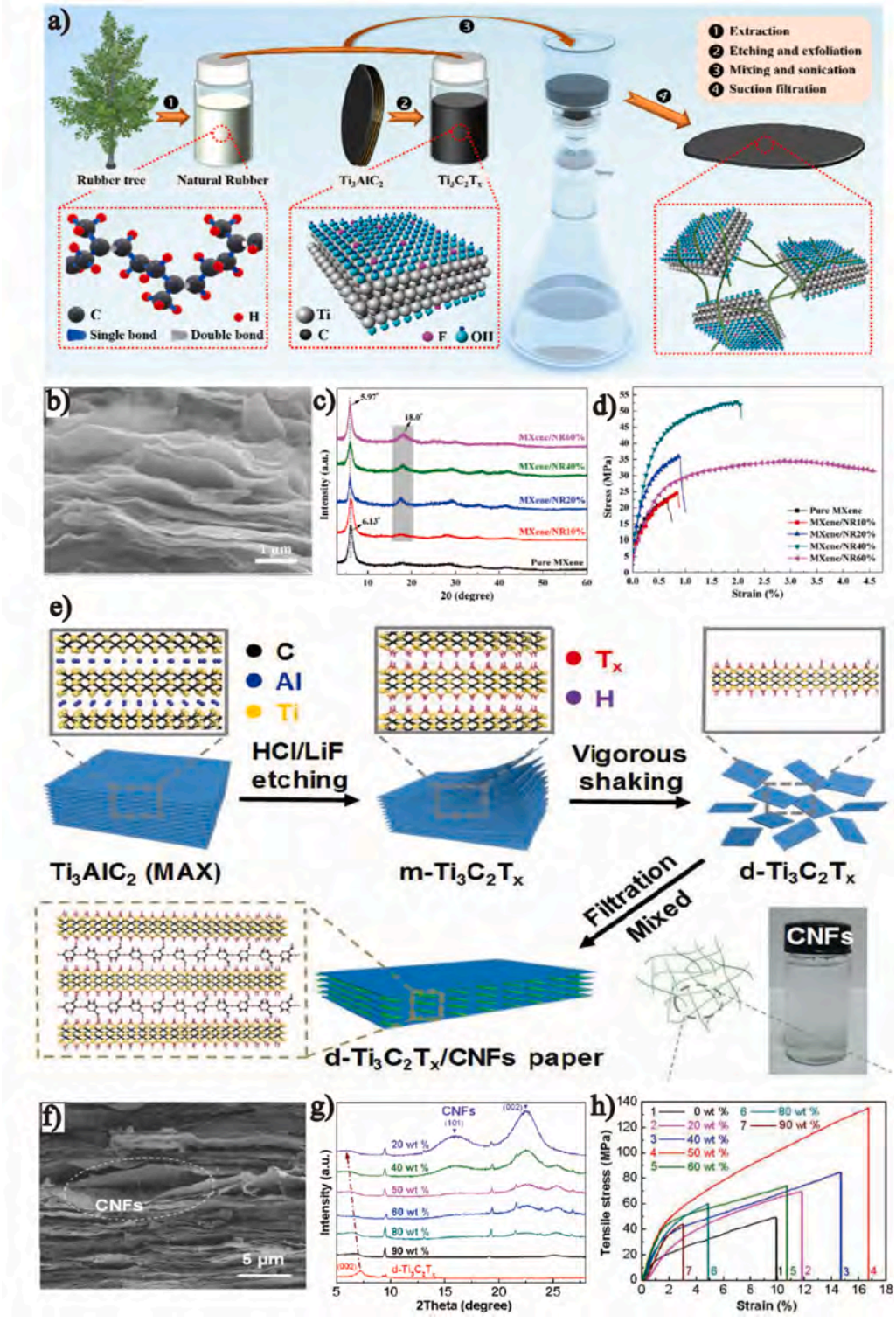

Fig. 8. (a) Schematic illustration of preparing MXene/NR composite film by vacuum filtration. Reprinted with permission.[45] Copyright 2020, Elsevier. (b) The cross-sectional SEM image of MXene/NR10%. Reprinted with permission.[45] Copyright 2020, Elsevier. (c) The XRD patterns of MXene/NR composite films with different NR addition. Reprinted with permission.[45] Copyright 2020, Elsevier. (d) The stress–strain curves of MXene/NR composite films with different NR addition. Reprinted with permission.[45] Copyright 2020, Elsevier. (e) Schematic illustration of preparing $Ti_3C_2T_x$/CNFs composite film. Reprinted with permission.[69] Copyright 2018, American Chemical Society. (f) The SEM image of the fracture surface of the $Ti_3C_2T_x$/CNFs composite film. Reprinted with permission.[69] Copyright 2018, American Chemical Society. (g) The XRD patterns of $Ti_3C_2T_x$/CNFs composite films with different $Ti_3C_2T_x$ content. Reprinted with permission.[69] Copyright 2018, American Chemical Society. (h) The stress–strain curves of $Ti_3C_2T_x$/CNFs composite films with different $Ti_3C_2T_x$ content. Reprinted with permission.[69] Copyright 2018, American Chemical Society.

section. When MXene content is 50%, optimal parameters are obtained such as tensile strength = 135.4 ± 6.9 MPa, fracture strain = 16.7 ± 0.7%, Young's modulus = 3.8 ± 0.3 GPa and bending number in the folding endurance test = 14260 times.

The mechanical properties of MXene films, such as tensile strength, fracture strain, and Young's modulus, are greatly strengthened by compounding with organic polymers, which is the most commonly used method at present. Concurrently, the introduction of polymer enlarges the interlayer spacing and enhances the integration between nanosheets, showing impressive volume capacitance and good electromagnetic shielding performance in flexible electronic devices. However, the above performance improvement is at the expense of MXenes' conductivity. It is an urgent problem to transform the weak interaction between nanosheets into high strength combinations while maintaining the excellent conducitivity of MXenes.

3.3.2. Compounding for stability enhancement and hydrophilicity regulation

By compounding with other materials, not only the mechanical properties of MXene films can be greatly enhanced, but also their stability and hydrophilicity can be changed. Metastable MXenes react readily with oxygen, which results in their structural degradation and loss of electrical conductivity, thus seriously limiting the development of MXene-based materials. To address this challenge, Wu's team [47] proposed an approach based on carbon nanoplating, whose capping effect and reducibility contributed to effective protection for pristine MXenes (Fig. 9a). Through hydrothermal carbonization and subsequent thermal carbonization, the carbon nanoplating was transformed from the glucose molecule adsorbed on MXene surface, while the Ti_3C_2 was also preserved during the whole hydrothermal reaction and annealing process. MoS_2 nanoplates were grown on the surface of MXene with and without the protection of carbon nanoplating to explore further the lithium storage and hydrogen evolution capabilities of this system (Fig. 9b) not detailed here. According to the XRD analysis results, the

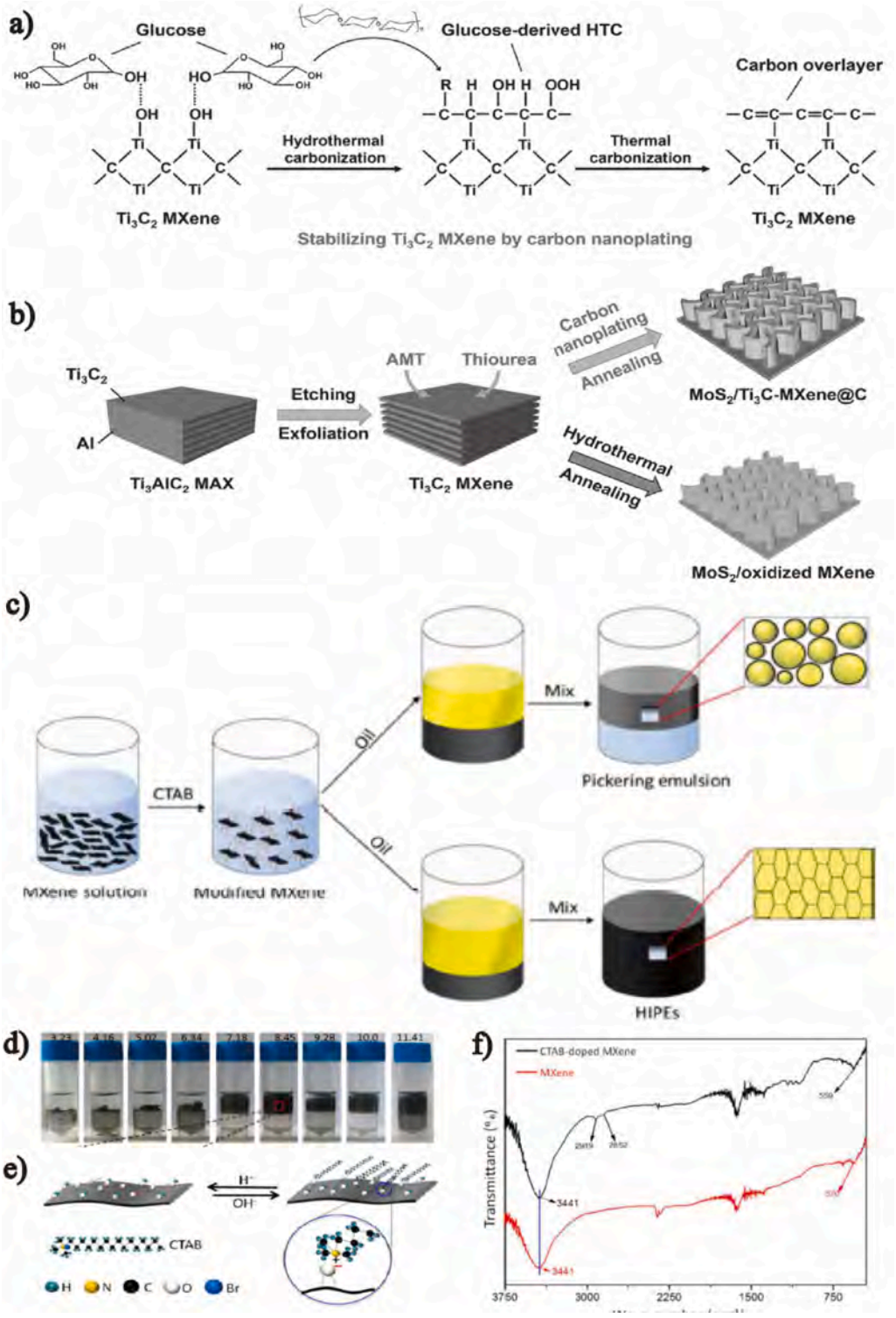

Fig. 9. (a) Schematic illustration of preparing carbon nanoplating on the surface of Ti_3C_2. This process involves the adsorption of glucose molecules, the formation of hydrothermal carbon, and thermal carbonization at high temperatures. Reprinted with permission.[47] Copyright 2017, Wiley-VCH. (b) The preparation process of MoS_2/Ti_3C_2-MXene@C and MoS_2/oxidized MXene hybrid systems. $Ti_3C_2T_x$ is rapidly transformed into TiO_2 during the reaction in the absence of carbon nanoplating. Reprinted with permission.[47] Copyright 2017, Wiley-VCH. (c) Schematic illustration of preparing oil-in-water Pickering emulsions and high internal phase Pickering emulsions (HIPEs) with CTAB-modified Ti_3C_2 (water molecules: blue, dodecane molecules: yellow). Reprinted with permission.[46] Copyright 2018, The Royal Society of Chemistry. (d) The effect of pH in an aqueous phase on emulsion stability with a fixed addition of CTAB and Ti_3C_2. Reprinted with permission.[46] Copyright 2018, The Royal Society of Chemistry. (e) The interaction between CTAB and Ti_3C_2 at different pH. Reprinted with permission.[46] Copyright 2018, The Royal Society of Chemistry. (f) The FTIR spectra of CTAB-modified Ti_3C_2. Reprinted with permission.[46] Copyright 2018, The Royal Society of Chemistry.

MoS_2/Ti_3C_2-MXene@C hybrid system shows the diffraction peak of disordered carbon, while the (1 0 1) peak of anatase TiO_2 appears in the MoS_2/oxidized MXene system. Furthermore, two characteristic peaks of Ti_3C_2 arise at 457.8 (2p3/2) and 463.6 eV (2p1/2) in Ti 2p XPS spectrum of the sample with nanoplating, which disappeared in oxidized samples demonstrating that Ti_3C_2 was protected by carbon nanoplating during the whole treatment process.

It is well known that the –OH termination introduced during synthesis endows MXenes with excellent hydrophilic character. To realize the three-dimensional assembly of Ti_3C_2 at the water/oil interface, Bian's study [46] tried to control their hydrophilic-hydrophobic character with the addition of a cationic activator (cetyltrimethylammonium bromide, CTAB) (Fig. 9c). The interaction between CTAB and surface termination of Ti_3C_2 is very sensitive to the pH of the aqueous phase, thus the hydrophobic transition can only be realized in neutral or alkaline conditions (Fig. 9d). The formation of stable emulsion implies that Ti_3C_2 was successfully modified by CTAB, which is attributed to the positively charged head ($-N(CH_3)_3$) in CTAB that replaced the hydrogen in [Ti-O]-H^+ group on Ti_3C_2 surface or formed ionically bond to the electronegative oxygen atoms in the Ti-O-Ti group. Interestingly, the Ti_3C_2 surface can be occupied reversibly by proton hydrogen or CTAB in acidic or alkaline environments (Fig. 9e). The Ti_3C_2 FTIR spectra before and after CTAB modification are provided in Fig. 9f. The Ti-O peak shift from 570 cm^{-1} to 559 cm^{-1}, and the appearance of two new peaks from the $–CH_2$ group in CTAB show the successful bonding of cationic activator to surface negatively charged site.

When compounding MXenes with other materials, the components are connected by various interactions such as covalent, ionic, and hydrogen bonds. The hybrid system shows the characteristics of each component at the same time, thus making up for the shortcomings of a single material and better meeting the needs of different applications. However, the disadvantage of this post-processing method is also very obvious, that is, the mixing of various materials brings property dilution for the individual component. Therefore, the trade-off between the properties from different components in the system is vital.

4. Application of MXenes' post-processing modification

Through various post-processing modification methods, the electrical, mechanical properties and environmental stability of MXenes can be adjusted, which promotes the application of energy storage, electromagnetic shielding, sensing and many other fields.

High conductivity and environmental stability are desired properties of MXens for many applications. Atomic doping and materials compounding are offen used to enhance these two properties of MXenes. In one example, nitrogen doped $Ti_3C_2T_x$ was prepared after annealing with ammonia in Wen's work, and the corresponding electrode obtained higher conductivity, which improves the electrochemical capacitance of supercapacitor [81]. In another work, the formation of nanoplating enhanced the oxygen resistance of MXenes, thus fabricating lithium storage and hydrogen evolution devices with high environmental stability [47].

Heat treatment is also an efeective approach to enhance the conductivity of MXene films. Besides, the interlayer spacing and microstructures can also be tuned by this method. For the thick Ti_3CNT_x films after heat treatment, the narrowing of interlayer spacing improves their conductivity, while the appearance of slit pores increases the reflection interface, endowing the whole structures with good electromagnetic shielding performance [32]. Liu et al. fabricated MXenes foam with the aid of hydrazine assistant, and the formation of porous structure was responsible for the high shielding efficiency [31].

Grafting or compounding with other materials will endue MXenes with more sening capabilities. The MXenes grafted with PDMAEMA have unique properties derived from termination, which can be used to sense various environmental factors such as temperature and gas content [42]. Compounding MXenes with other low dimensional materials such as graphene can expand their interlayer spacing and change the stacking mode and bonding strength, which is widely used in fabricating flexible force sensors and many other fields [36,82].

5. Conclusions and outlook

Herein, the latest post-processing approaches for MXenes, including atomic doping, termination changing, and materials compounding, are comprehensively reviewed. Through these post-treatments, the electrical, mechanical properties and environmental stability of MXenes can be optimized, which is favarble for the applications in energy storage, electromagnetic shielding, and flexible sensors.

Despite the inspiring progress achieved so far, significant challenges remain. First of all, the researches dealing with doping MXenes are relatively less, and the internal mechanism has not been fully elucidated. As an important post-processing approach, the influence of atomic doping on MXenes properties is not limited to conductivity. It has been confirmed in recent studies [83] that the 2D materials can be stabilized by atomic doping. Second, although MXenes with local termination-free have been reported [29], this state is very unstable and surface terminations are necessary. The key to customize MXenes properties is the accurate control of intrinsic functional groups through post-treatment processing. It is also a challenge to explore the corresponding external termination grafting, which can complement the required MXenes properties, thus meeting the needs of different applications. Finally, compounding MXenes with other materials inevitably brings the dilution of their own properties. It is urgent to find a hybrid system that is able to make a strong interaction with nanosheets and significantly improve MXenes properties through a small amount of additives. Another perspective is to explore different processing combinations of MXenes like 3D printing and laser integration to post-process MXenes with simultaneous compounding with polymers [84]. It is foreseeable that MXenes with targeted mechanical and electrical properties will play a full role in the application of energy, environmental, and electronic fields.

Declaration of Competing Interest

The authors declare that they have no known competing financial interests or personal relationships that could have appeared to influence the work reported in this paper.

Acknowledgements

This work was supported by the National Key Research and Development Program of China (2016YFA0203000), the National Natural Science Foundation of China (Grant No.61871368), the Instrument and Equipment Development Program Sponsored by CAS (YJKYYQ20180065), the Youth Innovation Promotion Association CAS, ES and RDR acknowledge the Russian Science Foundation grant (project number 19-75-10046) and the Shanghai science committee (19DZ1202601).

References

[1] M. Naguib, V.N. Mochalin, M.W. Barsoum, Y. Gogotsi, 25th anniversary article: MXenes: a new family of two-dimensional materials, Adv. Mater. 26 (7) (2014) 992–1005, https://doi.org/10.1002/adma.201304138.

[2] K.S. Novoselov, A.K. Geim, S.V. Morozov, D. Jiang, Y. Zhang, S.V. Dubonos, I. V. Grigorieva, A.A. Firsov, Electric field effect in atomically thin carbon films, Science 306 (5696) (2004) 666–669, https://doi.org/10.1126/science.1102896.

[3] K.S. Novoselov, D. Jiang, F. Schedin, T.J. Booth, V.V. Khotkevich, S.V. Morozov, A. K. Geim, Two-dimensional atomic crystals, PNAS 102 (30) (2005) 10451–10453, https://doi.org/10.1073/pnas.0502848102.

[4] J.N. Coleman, M. Lotya, A. O'Neill, S.D. Bergin, P.J. King, U. Khan, K. Young, A. Gaucher, S. De, R.J. Smith, I.V. Shvets, S.K. Arora, G. Stanton, H.-Y. Kim, K. Lee, G.T. Kim, G.S. Duesberg, T. Hallam, J.J. Boland, J.J. Wang, J.F. Donegan, J. C. Grunlan, G. Moriarty, A. Shmeliov, R.J. Nicholls, J.M. Perkins, E.M. Grieveson, K. Theuwissen, D.W. McComb, P.D. Nellist, V. Nicolosi, Two-dimensional

nanosheets produced by liquid exfoliation of layered materials, Science 331 (6017) (2011) 568–571, https://doi.org/10.1126/science.1194975.
[5] M. Naguib, M. Kurtoglu, V. Presser, J. Lu, J. Niu, M. Heon, L. Hultman, Y. Gogotsi, M.W. Barsoum, Two-dimensional nanocrystals produced by exfoliation of Ti3AlC2, Adv. Mater. 23 (37) (2011) 4248–4253, https://doi.org/10.1002/adma.201102306.
[6] Y. Gogotsi, Q. Huang, MXenes: two-dimensional building blocks for future materials and devices, ACS Nano 15 (4) (2021) 5775–5780, https://doi.org/10.1021/acsnano.1c03161.
[7] M.W. Barsoum, T. El-Raghy, The MAX phases: unique new carbide and nitride materials - ternary ceramics turn out to be surprisingly soft and machinable, yet also heat-tolerant, strong and lightweight, Am. Sci. 89 (4) (2001) 334–343, https://doi.org/10.1511/2001.4.334.
[8] M.W. Barsoum, The M(N+1)AX(N) phases: a new class of solids: thermodynamically stable nanolaminates, Prog. Solid State Chem. 28 (1–4) (2000) 201–281, https://doi.org/10.1016/s0079-6786(00)00006-6.
[9] J.L. Hart, K. Hantanasirisakul, A.C. Lang, B. Anasori, D. Pinto, Y. Pivak, J.T. van Omme, S.J. May, Y. Gogotsi, M.L. Taheri, Control of MXenes' electronic properties through termination and intercalation, Nat. Commun. 10 (1) (2019), https://doi.org/10.1038/s41467-018-08169-8.
[10] M. Malaki, A. Maleki, R.S. Varma, MXenes and ultrasonication, J. Mater. Chem. A 7 (18) (2019) 10843–10857, https://doi.org/10.1039/c9ta01850f.
[11] M. Ghidiu, M.R. Lukatskaya, M.-Q. Zhao, Y. Gogotsi, M.W. Barsoum, Conductive two-dimensional titanium carbide 'clay' with high volumetric capacitance, Nature 516 (7529) (2014) 78–U171, https://doi.org/10.1038/nature13970.
[12] Z. Ling, C.E. Ren, M.-Q. Zhao, J. Yang, J.M. Giammarco, J. Qiu, M.W. Barsoum, Y. Gogotsi, Flexible and conductive MXene films and nanocomposites with high capacitance, PNAS 111 (47) (2014) 16676–16681, https://doi.org/10.1073/pnas.1414215111.
[13] J. Xuan, Z. Wang, Y. Chen, D. Liang, L. Cheng, X. Yang, Z. Liu, R. Ma, T. Sasaki, F. Geng, Organic-base-driven intercalation and delamination for the production of functionalized titanium carbide nanosheets with superior photothermal therapeutic performance, Angewandte Chemie-International Edition 55 (47) (2016) 14569–14574, https://doi.org/10.1002/anie.v55.4710.1002/anie.201606643.
[14] T. Li, L. Yao, Q. Liu, J. Gu, R. Luo, J. Li, X. Yan, W. Wang, P. Liu, B. Chen, W. Zhang, W. Abbas, R. Naz, D.i. Zhang, Fluorine-free synthesis of high-purity Ti3C2Tx (T=OH, O) via alkali treatment, Angewandte Chemie-International Edition 57 (21) (2018) 6115–6119, https://doi.org/10.1002/anie.v57.2110.1002/anie.201800887.
[15] A. Jawaid, A. Hassan, G. Neher, D. Nepal, R. Pachter, W.J. Kennedy, S. Ramakrishnan, R.A. Vaia, Halogen Etch of Ti3AlC2 MAX phase for MXene fabrication, ACS Nano 15 (2) (2021) 2771–2777, https://doi.org/10.1021/acsnano.0c0863010.1021/acsnano.0c08630.s001.
[16] W. Sun, S.A. Shah, Y. Chen, Z. Tan, H. Gao, T. Habib, M. Radovic, M.J. Green, Electrochemical etching of Ti2AlC to Ti2CTx (MXene) in low-concentration hydrochloric acid solution, J. Mater. Chem. A 5 (41) (2017) 21663–21668, https://doi.org/10.1039/c7ta05574a.
[17] S. Yang, P. Zhang, F. Wang, A.G. Ricciardulli, M.R. Lohe, P.W.M. Blom, X. Feng, Fluoride-free synthesis of two-dimensional titanium carbide (MXene) using a binary aqueous system, Angewandte Chemie-International Edition 57 (47) (2018) 15491–15495, https://doi.org/10.1002/anie.v57.4710.1002/anie.201809662.
[18] P. Urbankowski, B. Anasori, T. Makaryan, D. Er, S. Kota, P.L. Walsh, M. Zhao, V. B. Shenoy, M.W. Barsoum, Y. Gogotsi, Synthesis of two-dimensional titanium nitride Ti4N3 (MXene), Nanoscale 8 (22) (2016) 11385–11391, https://doi.org/10.1039/c6nr02253g.
[19] C.J. Zhang, S. Pinilla, N. McEvoy, C.P. Cullen, B. Anasori, E. Long, S.-H. Park, A. Seral-Ascaso, A. Shmeliov, D. Krishnan, C. Morant, X. Liu, G.S. Duesberg, Y. Gogotsi, V. Nicolosi, Oxidation stability of colloidal two-dimensional titanium carbides (MXenes), Chem. Mater. 29 (11) (2017) 4848–4856, https://doi.org/10.1021/acs.chemmater.7b0074510.1021/acs.chemmater.7b00745.s00110.1021/acs.chemmater.7b00745.s002.
[20] O. Mashtalir, M. Naguib, V.N. Mochalin, Y. Dall'Agnese, M. Heon, M.W. Barsoum, Y. Gogotsi, Intercalation and delamination of layered carbides and carbonitrides, Nat. Commun. 4 (1) (2013), https://doi.org/10.1038/ncomms2664.
[21] M. Naguib, R.R. Unocic, B.L. Armstrong, J. Nanda, Large-scale delamination of multi-layers transition metal carbides and carbonitrides "MXenes", Dalton Trans. 44 (20) (2015) 9353–9358, https://doi.org/10.1039/c5dt01247c.
[22] H. Tang, Y. Yang, R. Wang, J. Sun, Improving the properties of 2D titanium carbide films by thermal treatment, J. Mater. Chem. C 8 (18) (2020) 6214–6220, https://doi.org/10.1039/c9tc07018d.
[23] M. Naguib, J. Come, B. Dyatkin, V. Presser, P.-L. Taberna, P. Simon, M. W. Barsoum, Y. Gogotsi, MXene: a promising transition metal carbide anode for lithium-ion batteries, Electrochem. Commun. 16 (1) (2012) 61–64, https://doi.org/10.1016/j.elecom.2012.01.002.
[24] M.R. Lukatskaya, S. Kota, Z. Lin, M.-Q. Zhao, N. Shpigel, M.D. Levi, J. Halim, P.-L. Taberna, M. Barsoum, P. Simon, Y. Gogotsi, Ultra-high-rate pseudocapacitive energy storage in two-dimensional transition metal carbides, Nature Energy 2 (8) (2017), https://doi.org/10.1038/nenergy.2017.105.
[25] X. Li, N.a. Li, Z. Huang, Z.e. Chen, G. Liang, Q.i. Yang, M. Li, Y. Zhao, L. Ma, B. Dong, Q. Huang, J. Fan, C. Zhi, Enhanced redox kinetics and duration of aqueous I-2/I- conversion chemistry by MXene confinement, Adv. Mater. 33 (8) (2021) 2006897, https://doi.org/10.1002/adma.v33.810.1002/adma.202006897.
[26] X. Li, M. Li, Z. Huang, G. Liang, Z. Chen, Q. Yang, Q. Huang, C. Zhi, Activating the I-0/I+ redox couple in an aqueous I-2-Zn battery to achieve a high voltage plateau, Energy Environ. Sci. 14 (1) (2021) 407–413, https://doi.org/10.1039/d0ee03086d.
[27] J. Ran, G. Gao, F.-T. Li, T.-Y. Ma, A. Du, S.-Z. Qiao, Ti3C2 MXene co-catalyst on metal sulfide photo-absorbers for enhanced visible-light photocatalytic hydrogen production, Nat. Commun. 8 (1) (2017), https://doi.org/10.1038/ncomms13907.
[28] L. Xiu, Z. Wang, M. Yu, X. Wu, J. Qiu, Aggregation-resistant 3D MXene-based architecture as efficient bifunctional electrocatalyst for overall water splitting, ACS Nano 12 (8) (2018) 8017–8028, https://doi.org/10.1021/acsnano.8b0284910.1021/acsnano.8b02849.s001.
[29] I. Persson, J. Halim, H. Lind, T.W. Hansen, J.B. Wagner, L.-Å. Näslund, V. Darakchieva, J. Palisaitis, J. Rosen, P.O.Å. Persson, 2D transition metal carbides (MXenes) for carbon capture, Adv. Mater. 31 (2) (2019) 1805472, https://doi.org/10.1002/adma.v31.210.1002/adma.201805472.
[30] F. Shahzad, M. Alhabeb, C.B. Hatter, B. Anasori, S.M. Hong, C.M. Koo, Y. Gogotsi, Electromagnetic interference shielding with 2D transition metal carbides (MXenes), Science 353 (6304) (2016) 1137–1140, https://doi.org/10.1126/science.aag2421.
[31] J. Liu, H.-B. Zhang, R. Sun, Y. Liu, Z. Liu, A. Zhou, Z.-Z. Yu, Hydrophobic, flexible, and lightweight mxene foams for high-performance electromagnetic-interference shielding, Adv. Mater. 29 (38) (2017), https://doi.org/10.1002/adma.201702367.
[32] A. Iqbal, F. Shahzad, K. Hantanasirisakul, M.-K. Kim, J. Kwon, J. Hong, H. Kim, D. Kim, Y. Gogotsi, C.M. Koo, Anomalous absorption of electromagnetic waves by 2D transition metal carbonitride Ti3CNTx (MXene), Science 369 (6502) (2020) 446–450, https://doi.org/10.1126/science:aba7977.
[33] X. Li, X. Yin, C. Song, M. Han, H. Xu, W. Duan, L. Cheng, L. Zhang, Self-assembly core-shell graphene-bridged hollow MXenes spheres 3D foam with ultrahigh specific EM absorption performance, Adv. Funct. Mater. 28 (41) (2018) 1803938, https://doi.org/10.1002/adfm.v28.4110.1002/adfm.201803938.
[34] X. Li, X. Yin, S. Liang, M. Li, L. Cheng, L. Zhang, 2D carbide MXene Ti2CTX as a novel high-performance electromagnetic interference shielding material, Carbon 146 (2019) 210–217, https://doi.org/10.1016/j.carbon.2019.02.003.
[35] X. Li, X. Yin, H. Xu, M. Han, M. Li, S. Liang, L. Cheng, L. Zhang, Ultralight MXene-coated interconnected sicnws three-dimensional lamellar foams for efficient microwave absorption in the X-band, Acs Appl. Mater. Interfaces 10 (40) (2018) 34524–34533, https://doi.org/10.1021/acsami.8b1365810.1021/acsami.8b13658.s001.
[36] Y. Yang, L. Shi, Z. Cao, R. Wang, J. Sun, Strain sensors with a high sensitivity and a wide sensing range based on a Ti3C2Tx (MXene) nanoparticle-nanosheet hybrid network, Adv. Funct. Mater. 29 (14) (2019) 1807882, https://doi.org/10.1002/adfm.v29.1410.1002/adfm.201807882.
[37] Y. Ma, N. Liu, L. Li, X. Hu, Z. Zou, J. Wang, S. Luo, Y. Gao, A highly flexible and sensitive piezoresistive sensor based on MXene with greatly changed interlayer distances, Nat. Commun. 8 (1) (2017), https://doi.org/10.1038/s41467-017-01136-9.
[38] H. An, T. Habib, S. Shah, H. Gao, M. Radovic, M.J. Green, J.L. Lutkenhaus, Surface-agnostic highly stretchable and bendable conductive MXene multilayers, Sci. Adv. 4 (3) (2018) eaaq0118, https://doi.org/10.1126/sciadv.aaq0118.
[39] S.J. Kim, H.-J. Koh, C.E. Ren, O. Kwon, K. Maleski, S.-Y. Cho, B. Anasori, C.-K. Kim, Y.-K. Choi, J. Kim, Y. Gogotsi, H.-T. Jung, Metallic Ti3C2TX MXene gas sensors with ultrahigh signal-to-noise ratio, ACS Nano 12 (2) (2018) 986–993, https://doi.org/10.1021/acsnano.7b0746010.1021/acsnano.7b07460.s001.
[40] B. Xu, M. Zhu, W. Zhang, X. Zhen, Z. Pei, Q. Xue, C. Zhi, P. Shi, Ultrathin MXene-micropattern-based field-effect transistor for probing neural activity, Adv. Mater. 28 (17) (2016) 3333–3339, https://doi.org/10.1002/adma.201504657.
[41] Z. Jin, Y. Fang, X. Wang, G. Xu, M. Liu, S. Wei, C. Zhou, Y. Zhang, Y. Xu, Ultra-efficient electromagnetic wave absorption with ethanol-thermally treated two-dimensional Nb2CTx nanosheets, J. Colloid Interf. Sci. 537 (2019) 306–315, https://doi.org/10.1016/j.jcis.2018.11.034.
[42] J. Chen, K. Chen, D. Tong, Y. Huang, J. Zhang, J. Xue, Q. Huang, T. Chen, CO2 and temperature dual responsive "Smart'' MXene phases, Chem. Commun. 51 (2) (2015) 314–317, https://doi.org/10.1039/c4cc07220k.
[43] L. Yang, C. Dall'Agnese, Y. Dall'Agnese, G. Chen, Y. Gao, Y. Sanehira, A.K. Jena, X.-F. Wang, Y. Gogotsi, T. Miyasaka, Surface-modified metallic Ti3C2Tx MXene as electron transport layer for planar heterojunction perovskite solar cells, Adv. Funct. Mater. 29 (46) (2019) 1905694, https://doi.org/10.1002/adfm.v29.4610.1002/adfm.201905694.
[44] F.M. Roemer, U. Wiedwald, T. Strusch, J. Halim, E. Mayerberger, M.W. Barsoum, M. Farle, Controlling the conductivity of Ti3C2 MXenes by inductively coupled oxygen and hydrogen plasma treatment and humidity, RSC Adv. 7 (22) (2017) 13097–13103, https://doi.org/10.1039/c6ra27505b.
[45] W. Yang, J.-J. Liu, L.-L. Wang, W. Wang, A.C.Y. Yuen, S. Peng, B. Yu, H.-D. Lu, G.H. Yeoh, C.-H. Wang, Multifunctional MXene/natural rubber composite films with exceptional flexibility and durability, Composites Part B-Engineering 188, 2020, https://doi.org/10.1016/j.compositesb.2020.107875.
[46] R. Bian, R. Lin, G. Wang, G. Lu, W. Zhi, S. Xiang, T. Wang, P.S. Clegg, D. Cai, W. Huang, 3D assembly of Ti3C2-MXene directed by water/oil interfaces, Nanoscale 10 (8) (2018) 3621–3625, https://doi.org/10.1039/c7nr07346a.
[47] X. Wu, Z. Wang, M. Yu, L. Xiu, J. Qiu, Stabilizing the MXenes by carbon nanoplating for developing hierarchical nanohybrids with efficient lithium storage and hydrogen evolution capability, Adv. Mater. 29 (24) (2017) 1607017, https://doi.org/10.1002/adma.201607017.
[48] I.R. Shein, A.L. Ivanovskii, Graphene-like titanium carbides and nitrides Tin+1Cn, Tin+1Nn (n=1, 2, and 3) from de-intercalated MAX phases: first-principles probing of their structural, electronic properties and relative stability, Comput. Mater. Sci. 65 (2012) 104–114, https://doi.org/10.1016/j.commatsci.2012.07.011.

[49] G.R. Berdiyorov, Effect of surface functionalization on the electronic transport properties of Ti3C2 MXene, EPL 111 (6) (2015) 67002, https://doi.org/10.1209/0295-5075/111/67002.
[50] Q. Tang, Z. Zhou, P. Shen, Are MXenes promising anode materials for Li ion batteries? computational studies on electronic properties and Li storage capability of Ti3C2 and Ti3C2X2 (X = F, OH) monolayer, J. Am. Chem. Soc. 134 (40) (2012) 16909–16916, https://doi.org/10.1021/ja308463r.
[51] Y. Xie, P.R.C. Kent, Hybrid density functional study of structural and electronic properties of functionalized Tin+1Xn (X = C, N) monolayers, Phys. Rev. B 87 (23) (2013), https://doi.org/10.1103/PhysRevB.87.235441.
[52] M.R. Lukatskaya, O. Mashtalir, C.E. Ren, Y. Dall'Agnese, P. Rozier, P.L. Taberna, M. Naguib, P. Simon, M.W. Barsoum, Y. Gogotsi, Cation intercalation and high volumetric capacitance of two-dimensional titanium carbide, Science 341 (6153) (2013) 1502–1505, https://doi.org/10.1126/science.1241488.
[53] Z. Guo, J. Zhou, C. Si, Z. Sun, Flexible two-dimensional Tin+1Cn (n=1, 2 and 3) and their functionalized MXenes predicted by density functional theories, PCCP 17 (23) (2015) 15348–15354, https://doi.org/10.1039/c5cp00775e.
[54] V.N Borysiuk, V.N Mochalin, Y. Gogotsi, Molecular dynamic study of the mechanical properties of two-dimensional titanium carbides Tin+1Cn (MXenes), Nanotechnology 26 (26) (2015) 265705, https://doi.org/10.1088/0957-4484/26/26/265705.
[55] P.G. Grützmacher, S. Suarez, A. Tolosa, C. Gachot, G. Song, B. Wang, V. Presser, F. Mücklich, B. Anasori, A. Rosenkranz, Superior wear-resistance of Ti3C2Tx multilayer coatings, ACS Nano 15 (5) (2021) 8216–8224, https://doi.org/10.1021/acsnano.1c0155510.1021/acsnano.1c01555.s002.
[56] B.C. Wyatt, A. Rosenkranz, B. Anasori, 2D MXenes: tunable mechanical and tribological properties, Adv. Mater. 33 (17) (2021) 2007973, https://doi.org/10.1002/adma.v33.1710.1002/adma.202007973.
[57] Y. Chae, S.J. Kim, S.-Y. Cho, J. Choi, K. Maleski, B.-J. Lee, H.-T. Jung, Y. Gogotsi, Y. Lee, C.W. Ahn, An investigation into the factors governing the oxidation of two-dimensional Ti3C2 MXene, Nanoscale 11 (17) (2019) 8387–8393, https://doi.org/10.1039/c9nr00084d.
[58] T. Hu, M. Hu, B. Gao, W. Li, X. Wang, Screening surface structure of MXenes by high-throughput computation and vibrational spectroscopic confirmation, J. Phys. Chem. C 122 (32) (2018) 18501–18509, https://doi.org/10.1021/acs.jpcc.8b0442710.1021/acs.jpcc.8b04427.s001.
[59] S. Huang, V.N. Mochalin, Hydrolysis of 2D transition-metal carbides (MXenes) in colloidal solutions, Inorg. Chem. 58 (3) (2019) 1958–1966, https://doi.org/10.1021/acs.inorgchem.8b0289010.1021/acs.inorgchem.8b02890.s001.
[60] T. Habib, X. Zhao, S.A. Shah, Y. Chen, W. Sun, H. An, J.L. Lutkenhaus, M. Radovic, M.J. Green, Oxidation stability of Ti3C2Tx MXene nanosheets in solvents and composite films, Npj 2d Materials and Applications, 3, 2019, https://doi.org/10.1038/s41699-019-0089-3.
[61] P. Urbankowski, B. Anasori, K. Hantanasirisakul, L. Yang, L. Zhang, B. Haines, S. J. May, S.J.L. Billinge, Y. Gogotsi, 2D molybdenum and vanadium nitrides synthesized by ammoniation of 2D transition metal carbides (MXenes), Nanoscale 9 (45) (2017) 17722–17730, https://doi.org/10.1039/c7nr06721f.
[62] C. Yang, Y. Tang, Y. Tian, Y. Luo, M.F.U. Din, X. Yin, W. Que, Flexible nitrogen-doped 2D titanium carbides (MXene) films constructed by an ex situ solvothermal method with extraordinary volumetric capacitance, Advanced Energy Materials, 8 (31), 2018, https://doi.org/10.1002/aenm.201802087.
[63] Y. Yoon, A.P. Tiwari, M. Choi, T.C. Novak, W. Song, H. Chang, T. Zyung, S.S. Lee, S. Jeon, K.-S. An, precious-metal-free electrocatalysts for activation of hydrogen evolution with nonmetallic electron donor: chemical composition controllable phosphorous doped vanadium carbide MXene, Advanced Functional Materials 29 (30), 2019, https://doi.org/10.1002/adfm.201903443.
[64] J. Li, D. Yan, S. Hou, Y. Li, T. Lu, Y. Yao, L. Pan, Improved sodium-ion storage performance of Ti3C2Tx MXenes by sulfur doping, J. Mater. Chem. A 6 (3) (2018) 1234–1243, https://doi.org/10.1039/c7ta08261d.
[65] M. Seredych, C.E. Shuck, D. Pinto, M. Alhabeb, E. Precetti, G. Deysher, B. Anasori, N. Kurra, Y. Gogotsi, High-temperature behavior and surface chemistry of carbide MXenes studied by thermal analysis, Chem. Mater. 31 (9) (2019) 3324–3332, https://doi.org/10.1021/acs.chemmater.9b0039710.1021/acs.chemmater.9b00397.s001.
[66] H. Wang, J. Zhang, Y. Wu, H. Huang, G. Li, X. Zhang, Z. Wang, Surface modified MXene Ti3C2 multilayers by aryl diazonium salts leading to large-scale delamination, Appl. Surf. Sci. 384 (2016) 287–293, https://doi.org/10.1016/j.apsusc.2016.05.060.
[67] J. Zhao, Y. Yang, C. Yang, Y. Tian, Y. Han, J. Liu, X. Yin, W. Que, A hydrophobic surface enabled salt-blocking 2D Ti3C2 MXene membrane for efficient and stable solar desalination, J. Mater. Chem. A 6 (33) (2018) 16196–16204, https://doi.org/10.1039/c8ta05569f.
[68] R. Liu, M. Miao, Y. Li, J. Zhang, S. Cao, X. Feng, Ultrathin biomimetic polymeric Ti3C2Tx MXene composite films for electromagnetic interference shielding, ACS Appl. Mater. Interfaces 10 (51) (2018) 44787–44795, https://doi.org/10.1021/acsami.8b1834710.1021/acsami.8b18347.s001.
[69] W.-T. Cao, F.-F. Chen, Y.-J. Zhu, Y.-G. Zhang, Y.-Y. Jiang, M.-G. Ma, F. Chen, Binary strengthening and toughening of MXene/Cellulose nanofiber composite paper with nacre-inspired structure and superior electromagnetic interference shielding properties, ACS Nano 12 (5) (2018) 4583–4593, https://doi.org/10.1021/acsnano.8b0099710.1021/acsnano.8b00997.s00110.1021/acsnano.8b00997.s00210.1021/acsnano.8b00997.s003.
[70] H. Riazi, M. Anayee, K. Hantanasirisakul, A.A. Shamsabadi, B. Anasori, Y. Gogotsi, M. Soroush, Surface modification of a mxene by an aminosilane coupling agent, Advanced Materials Interfaces, 7(6), 2020, https://doi.org/10.1002/admi.201902008.
[71] R.B. Rakhi, B. Ahmed, M.N. Hedhili, D.H. Anjum, H.N. Alshareef, Effect of Postetch annealing gas composition on the structural and electrochemical properties of Ti2CTx MXene electrodes for supercapacitor applications, Chem. Mater. 27 (15) (2015) 5314–5323, https://doi.org/10.1021/acs.chemmater.5b01623.
[72] A. Rosenkranz, P.G. Gruetzmacher, R. Espinoza, V.M. Fuenzalida, E. Blanco, N. Escalona, F.J. Gracia, R. Villarroel, L. Guo, R. Kang, F. Muecklich, S. Suarez, Z. Zhang, Multi-layer Ti3C2Tx-nanoparticles (MXenes) as solid lubricants - role of surface terminations and intercalated water, Appl. Surf. Sci. 494 (2019) 13–21, https://doi.org/10.1016/j.apsusc.2019.07.171.
[73] N.C. Osti, M. Naguib, A. Ostadhossein, Y. Xie, P.R.C. Kent, B. Dyatkin, G. Rother, W.T. Heller, A.C.T. van Duin, Y. Gogotsi, E. Mamontov, Effect of metal ion intercalation on the structure of mxene and water dynamics on its internal surfaces, Acs Applied Materials & Interfaces, 8(14), 2016, 8859-8863, https://doi.org/10.1021/acsami.6b01490.
[74] Y. Jiang, T. Sun, X. Xie, W. Jiang, J. Li, B. Tian, C. Su, Oxygen-functionalized ultrathin Ti3C2Tx mxene for enhanced electrocatalytic hydrogen evolution, ChemSusChem 12 (7) (2019) 1368–1373, https://doi.org/10.1002/cssc.v12.710.1002/cssc.201803032.
[75] J.-Q. Luo, S. Zhao, H.-B. Zhang, Z. Deng, L. Li, Z.-Z. Yu, Flexible, stretchable and electrically conductive MXene/natural rubber nanocomposite films for efficient electromagnetic interference shielding, Compos. Sci. Technol. 182 (2019) 107754, https://doi.org/10.1016/j.compscitech.2019.107754.
[76] Z. Zhang, S. Yang, P. Zhang, J. Zhang, G. Chen, X. Feng, Mechanically strong MXene/Kevlar nanofiber composite membranes as high-performance nanofluidic osmotic power generators, Nat. Commun. 10 (1) (2019), https://doi.org/10.1038/s41467-019-10885-8.
[77] F. Xie, F. Jia, L. Zhuo, Z. Lu, L. Si, J. Huang, M. Zhang, Q. Ma, Ultrathin MXene/aramid nanofiber composite paper with excellent mechanical properties for efficient electromagnetic interference shielding, Nanoscale 11 (48) (2019) 23382–23391, https://doi.org/10.1039/c9nr07331k.
[78] S. Jiao, A. Zhou, M. Wu, H. Hu, Kirigami patterning of MXene/bacterial cellulose composite paper for all-solid-state stretchable micro-supercapacitor arrays, Adv. Sci. 6 (12) (2019) 1900529, https://doi.org/10.1002/advs.v6.1210.1002/advs.201900529.
[79] L. Li, N. Zhang, M. Zhang, X. Zhang, Z. Zhang, Flexible Ti3C2Tx/PEDOT:PSS films with outstanding volumetric capacitance for asymmetric supercapacitors, Dalton Trans. 48 (5) (2019) 1747–1756, https://doi.org/10.1039/c8dt04374d.
[80] H. Xu, D. Zheng, F. Liu, W. Li, J. Lin, Synthesis of an MXene/polyaniline composite with excellent electrochemical properties, J. Mater. Chem. A 8 (12) (2020) 5853–5858, https://doi.org/10.1039/d0ta00572j.
[81] Y. Wen, T.E. Rufford, X. Chen, N. Li, M. Lyu, L. Dai, L. Wang, Nitrogen-doped Ti3C2Tx MXene electrodes for high-performance supercapacitors, Nano Energy 38 (2017) 368–376, https://doi.org/10.1016/j.nanoen.2017.06.009.
[82] Y. Zhang, L. Wang, L. Zhao, K. Wang, Y. Zheng, Z. Yuan, D. Wang, X. Fu, G. Shen, W. Han, Flexible self-powered integrated sensing system with 3D periodic ordered black phosphorus@MXene thin-films, Advanced Materials, 33(22), 2021, https://doi.org/10.1002/adma.202007890.
[83] Z. Du, S. Yang, S. Li, J. Lou, S. Zhang, S. Wang, B. Li, Y. Gong, L. Song, X. Zou, P.M. Ajayan, Conversion of non-van der Waals solids to 2D transition-metal chalcogenides, Nature 577(7791), 2020, 492-+. https://doi.org/10.1038/s41586-019-1904-x.
[84] R.D. Rodriguez, S. Shchadenko, G. Murastov, A. Lipovka, M. Fatkullin, I. Petrov, T.-H. Tran, A. Khalelov, M. Saqib, N.E. Villa, V. Bogoslovskiy, Y. Wang, C.-G. Hu, A. Zinovyev, W. Sheng, J.-J. Chen, I. Amin, E. Sheremet, Ultra-robust flexible electronics by laser-driven polymer-nanomaterials integration, Advanced Functional Materials 31(17), 2021, https://doi.org/10.1002/adfm.202008818.